UC Irvine
UC Irvine Previously Published Works

Title

Seasonal Sources of Whole-Lake CH4 and CO2 Emissions From Interior Alaskan Thermokarst Lakes

Permalink

https://escholarship.org/uc/item/8qz3j1b6

Journal

Journal of Geophysical Research Biogeosciences, 124(5)

ISSN

2169-8953

Authors

Elder, CD
Schweiger, M
Lam, B
et al.

Publication Date

2019-05-01

DOI

10.1029/2018jg004735

Peer reviewed

Seasonal Sources of Whole-Lake CH_4 and CO_2 Emissions From Interior Alaskan Thermokarst Lakes

C. D. Elder[1,2] , M. Schweiger[1] , B. Lam[1], E. D. Crook[1], X. Xu[1] , J. Walker[1], K. M. Walter Anthony[3], and C. I. Czimczik[1]

[1]Department of Earth System Science, University of California, Irvine, CA, USA, [2]Now at Jet Propulsion Laboratory, California Institute of Technology, Pasadena, CA, USA, [3]Water and Environmental Research Center, University of Alaska Fairbanks, Fairbanks, AK, USA

Abstract The lakes that form via ice-rich permafrost thaw emit CH_4 and CO_2 to the atmosphere from previously frozen ancient permafrost sources. Despite this potential to positively feedback to climate change, lake carbon emission sources are not well understood on whole-lake scales, complicating upscaling. In this study, we used observations of radiocarbon (^{14}C) and stable carbon (^{13}C) isotopes in the summer and winter dissolved CH_4 and CO_2 pools, ebullition-CH_4, and multiple independent mass balance approaches to characterize whole-lake emission sources and apportion annual emission pathways. Observations focused on five lakes with variable thermokarst in interior Alaska. The ^{14}C age of discrete ebullition-CH_4 seeps ranged from 395 ± 15 to 28,240 ± 150 YBP across all study lakes; however, dissolved [14]CH_4 was younger than 4,730 YBP. In the primary study lake, Goldstream L., the integrated whole-lake ^{14}C age of ebullition-CH_4, as determined by three different approaches, ranged from 3,290 to 6,740 YBP. A new dissolved-^{14}C-CH_4-based approach to estimating ebullition ^{14}C age and flux showed close agreement to previous ice-bubble surveys and bubble-trap flux estimates. Differences in open water versus ice-covered dissolved gas concentrations and their ^{14}C and ^{13}C isotopes revealed the influence of winter ice trapping and forcing ebullition-CH_4 into the underlying water column, where it comprised 50% of the total dissolved CH_4 pool by the end of winter. Across the study lakes, we found a relationship between the whole-lake ^{14}C age of dissolved CH_4 and CO_2 and the extent of active thermokarst, representing a positive feedback system that is sensitive to climate warming.

Plain Language Summary Lakes that form as a result of thawing permafrost (perennially frozen ground) can release new greenhouse gases from ancient carbon reservoirs, which further warm the atmosphere and promote more permafrost thaw. Existing observations of this phenomenon are insufficient to fully understand the impact that thaw lakes have on the current atmosphere, let alone the atmosphere of a future warmer world. In this study, we used a novel approach and made open water and ice-covered measurements of rare carbon isotopes in methane and carbon dioxide dissolved in lake water and in bubbles emitted from sediments to determine the whole-lake-scale environmental drivers that regulate gas emissions from thawing permafrost. We learned that despite highly variable carbon source ages within single lakes, the presence of winter-ice traps and mixes all lake sources proportionally into the dissolved gas pool during winter and allows the stronger greenhouse gas, methane, to be oxidized to carbon dioxide before emission to the atmosphere in spring. This study also confirmed that higher levels of permafrost thaw within a lake are related to older carbon sources fueling whole-lake gas emissions, which, if consistent with lakes across northern permafrost regions, is evidence of a potential positive feedback to further climate warming.

1. Introduction

Thermokarst lakes, formed by thaw and subsidence of ice-rich permafrost, are a globally significant source of the greenhouse gases (GHG), methane (CH_4), and carbon dioxide (CO_2), to the atmosphere (Wik, Varner, et al., 2016). Although various studies have focused on the magnitude of these carbon (C) fluxes (Elder et al., 2018; Kling et al., 1991; Sepulveda-Jauregui et al., 2015), the environmental processes and sources that contribute to whole-lake CH_4 and CO_2 emissions are not well understood on broad spatial or seasonal scales, making future pan-Arctic emission projections highly uncertain (Walter Anthony et al., 2016). As the climate in permafrost regions is expected to warm more rapidly than anywhere on Earth in the next 100 years (Serreze & Barry, 2011), there is an urgent need to understand the annual and seasonal dynamics of CH_4 and

CO_2 production, processing, and emission on whole-lake scales in climate-sensitive thermokarst lakes (Denfeld et al., 2018).

In yedoma (ice and C-rich eolian sediment of the Pleistocene-aged mammoth steppe ecosystem), thermokarst lake formation is known to liberate ancient, previously frozen organic carbon (C) to microbial decomposition (Walter Anthony et al., 2016; Zimov et al., 1997), which produces CH_4 and CO_2 under anaerobic conditions. If thermokarst lakes mobilize large quantities of ancient permafrost C to the atmosphere, they could encourage a significant positive feedback to climate warming (Walter et al., 2006). The magnitude of this feedback will depend not only on the rate but also on the chemical species and source of C released (Elder et al., 2018). Carbon emissions in the form of CH_4 have a greater impact on climate, because CH_4 is 30 times more powerful than CO_2 as a GHG on a 100-year timescale (Myhre et al., 2013). Emissions sourced from ancient C deposited during the ice age conditions of the late Pleistocene (11,500 to ~50,000 YBP; Murton et al., 2015) have a greater warming feedback potential than emissions sourced from C that was only recently CO_2 in the atmosphere because they represent a net addition to the active carbon cycle. This is similar to fossil fuel emissions, where flux of ancient C (as GHGs) to the modern atmosphere perturbs the Earth system, forcing disequilibria in the global radiative balance and C cycle.

Determining annual emissions of CH_4 and CO_2 from thermokarst lakes is challenging since the gases (especially CH_4) are emitted via several pathways, including diffusion, ebullition, plant-mediated transport, and ice-bubble storage, all with variable rates depending on the time of year (Greene et al., 2014). Ebullition is thought to be the dominant mode of CH_4 emission from yedoma thermokarst lakes (Sepulveda-Jauregui et al., 2015); however, diffusive fluxes can dominate in larger nonthermokarst lakes (Bastviken et al., 2004) or some peatland thermokarst lakes (Matveev et al., 2016). Additionally, the C sources for ebullitive CH_4 and CO_2 can vary in mean age by tens of thousands of years within a single lake (Brosius et al., 2012; Walter et al., 2008). Together, the large spatial and temporal heterogeneity of emission pathways and C sources complicate observation strategies for upscaling ancient permafrost C losses on the regional level.

To address heterogeneity, this study took advantage of winter ice cover and quantified seasonal changes in the amount and isotopic composition of CH_4 and CO_2 dissolved in thermokarst lakes to estimate C emission sources and pathways on a whole-lake and annual basis. During winter, emissions are inhibited beneath lake ice and CH_4 and CO_2 from all lake sources and pathways are forced to mix into the unfrozen water column (Greene et al., 2014). As a result, the isotopic signatures of dissolved CH_4 and CO_2 during winter are proportional to the strongest sources fueling gas production. Specifically, we used open water and ice-covered measurements of the concentration, stable C isotope (^{13}C), and radiocarbon (^{14}C) content of CH_4 and CO_2 dissolved in lake water and emitted by ebullition from thermokarst lakes in central Alaska to investigate the following questions: (1) How do the dissolved pools of CH_4 and CO_2 integrate whole-lake emission sources and pathways on an annual basis? (2) How does lake morphology (size and depth) and expansion rate influence the C sources and emission pathways? Our unique approach facilitates lake-to-lake comparisons, understanding of the environmental drivers of thermokarst C emissions, and observation of lake-CH_4 and CO_2 emissions on scales relevant for regional analysis.

2. Materials and Methods

2.1. Study Region and Lakes

We investigated the sources of CH_4 and CO_2 emissions in five thermokarst-affected lakes located on private land, within 30 km of Fairbanks in interior Alaska from April 2015 to March 2016. Here many lakes (including at least four of the five study lakes) formed via thermokarst or are today affected by thermokarst along one or more shorelines. The study region is in the discontinuous permafrost zone, with continental climate characterized by a mean annual air temperature of −2.4 °C and annual precipitation of 274 mm (Fairbanks Int. Airport, 1981–2010, U.S. National Climatic Data Center) and boreal forest vegetation.

The lakes are situated upland of the Tanana and Chena Rivers, in complex quaternary deposits formed by alternating cycles of silt and gravel deposition and erosion and permafrost formation and degradation (Muhs & Budahn, 2006). Our five study lakes are situated in Pleistocene yedoma-type, organic-and-ice-rich deposits of the Gold Hill and Goldstream loess formations (Table 1). Due to logistical limitations and inaccessibility of some field sites, we primarily focused on Goldstream Lake (GSL), where previous work

Table 1
Physical Properties of Study Lakes

Lake[a]	Lat. °N	Long. °W	Surface area km^2	Max. known depth m	Permafrost soil type[c]	Active thermokarst	Estimated age calendar years
Goldstream[b]	64.916	147.847	0.010	4.7	yedoma	moderate	>120
Vault[b]	65.029	147.699	0.003	4.6	yedoma	major	400
Cranberry	64.936	147.821	0.006	11.5	yedoma	minor	unknown
Doughnut[b]	64.899	147.908	0.034	3.8	non-yedoma	insignificant	1,000
Smith[b]	64.865	147.868	0.094	4.4	non-yedoma	insignificant	>100

[a]Unoffical names. [b]Physical lake properties from (Sepulveda-Jauregui et al., 2015). [c]Yedoma refers to late Pleistocene loess deposits of organic- and ice-rich silt.

has characterized seasonal CH$_4$ dynamics, including ebullition and diffusive flux rates (Greene et al., 2014; Lindgren et al., 2016; Sepulveda-Jauregui et al., 2015; Walter Anthony & Anthony, 2013), seasonal dissolved CH$_4$ oxidation (Martinez-Cruz et al., 2015), permafrost and lake cycle dynamics (Brosius et al., 2012), and processing of dissolved organic C from thawing permafrost (Walter Anthony et al., 2016). Although sampling frequency fluctuated in our study lakes and some lakes were only sampled once or twice in a given season, mass balance calculations and modeled results are solely based on GSL, where observations were frequent enough to generate an estimate of uncertainty in our conclusions.

Goldstream Lake is actively eroding into yedoma permafrost primarily along its eastern margin and to a lesser extent on its southern margin. Altogether, less than 50% of GSL's shoreline is actively expanding. Based on extrapolation from remote sensing analysis, GSL is likely older than 120 years (Walter Anthony & Anthony, 2013). Vault Lake, approximately 400 years old, is actively eroding into yedoma permafrost, especially along the steep margins surrounding more than half the lake (Heslop et al., 2015). Additionally, significant organic-rich silt flows along the top of the active layer and in between tussocks have been observed adding sediment to the lake. Cranberry Lake shows minor erosion into yedoma permafrost, and remote sensing analysis indicates relatively stable shorelines, with minimal expansion during the last 60 years. Doughnut Lake has not expanded significantly during the last 60 years and is approximately 1,000 years old based on ^{14}C dating of a dead standing tree near the center of the lake (Sepulveda-Jauregui et al., 2015). Smith Lake has also not expanded and, based on historical maps, is older than 100 years. The extent of wetland plant coverage in Smith Lake appears to vary over time; however, the overall lake area appears stable. Minor expansion does occur in a small bay and is eroding into Holocene-aged peat deposits (Walter Anthony et al., 2016).

2.2. Collection of CO$_2$ and CH$_4$ in the Field
2.2.1. Collection of CH$_4$ and CO$_2$ From Beneath Floating Ice in Winter
During two consecutive winters (2014/2015 and 2015/2016), we collected CH$_4$ and CO$_2$ in ebullition gas and/or dissolved in lake water under floating ice (Table 2). For ebullition sampling, bubble traps were submerged and ebullition gas displaced lake water as it flowed into inverted, water-filled serum vials. This method is described in detail in Walter et al. (2008) and Walter Anthony et al. (2012).

Dissolved gas was collected in April 2015 just below the ice and at the lakebed at two locations on GSL and one location on Cranberry Lake ($n = 2$–4 per lake). In March 2016, we collected dissolved gases in three lakes ($n = 1$–8 per lake). At GSL, water was collected across an active thermokarst transect. In other lakes, samples were collected near their geographic centers to minimize potential bias from any particular shoreline and since thermokarst gradients were not as clearly defined as in GSL. To collect water samples for isotope analysis of dissolved gas, a hole was cut into floating ice with a chainsaw, and 1.4 L per sample of water from the ice/water interface was collected without headspace in polyethylene terephthalate (PETE) bottles with high-density polyethylene (HDPE) screw caps (342040-1000, Thermo Scientific, Waltham, MA, USA). For bottom-water samples, a Van Dorne bottle was used to collect water from near the lakebed. Prior to sampling, all sample bottles and screw caps were soaked in 1N HCl for 30 min and then rinsed with Milli-Q water. Since the PETE bottles allow for expansion and contraction, water samples were preserved by freezing until analysis. All samples were shipped to UC Irvine and analyzed within 9 months.

Table 2
Summary of Winter and Summer Sampling in Study Lakes

		Winter 2014/2015					Summer 2015					Winter 2015/2016				
		G	D	C	S	V	G	D	C	S	V	G	D	C	S	V
Dissolved																
[CH$_4$]	μM	482* (50)	-	-	-	-	354.7 (610.0)	2.7 (1.6)	-	2.5 (1.4)	574.2 (657.3)	458.1 (46.2)	363.9 (12.9)	-	12.3 (1.2)	-
[CO$_2$]	μM	-	-	-	-	-	614.9 (155.3)	657.9 (31.5)	-	855.2 (19.3)	1987.9 (1496.4)	638.7 (141.3)	671.0 (94.7)	-	170.1 (17.0)	-
δ^{13}CH$_4$	‰	-66.3 (4.3)	-	-61.7 (6.6)	-	-	-42.4 (5.4)	-35.5 (11.7)	-	-38.6 (18.8)	-58.8 (14.9)	-70.1 (0.3)	-69.8 (0.9)	-	-	-
δ^{13}CO$_2$	‰	-16.3 (0.2)	-	-16.2 (0.1)	-	-	-17.3 (0.5)	-16.6 (0.5)	-	-21.1 (0.5)	-28.4 (20.9)	-17.9 (0.5)	-18.2 (0.5)	-	-22.6 (0.5)	-
age CH$_4$	YBP	2692 (1,390)	-	390 (35)	-	-	921 (79)	75 (395)	-	0 (114)	3287 (229)	2161 (171)	808 (377)	-	0 (30)	-
age CO$_2$	YBP	949 (242)	-	0 (25)	-	-	677 (22)	0 (4)	-	0 (12)	2391 (764)	1392 (13)	28 (62)	-	0 (30)	-
n		4	-	2	-	-	10	4	-	4	4	8	3	-	1	-
Ebullition																
[CH$_4$]	%	-	-	-	-	-	44.8† (24.4)	-	57.1 (29.8)	75.6 (7.6)	77.2 (11.8)	93.7 (9.4)	-	-	-	-
[CO$_2$]	%	-	-	-	-	-	1.2 (0.6)	-	1.7 (0.1)	1.3 (0.1)	1.6 (0.6)	2.1 (0.2)	-	-	-	-
δ^{13}CH$_4$	‰	-	-	-	-	-	-72.1 (2.5)	-	-70.9 (3.7)	-63.9 (0.3)	-73.9 (5.9)	-77.4 (0.3)	-	-	-	-
δ^{13}CO$_2$	‰	-	-	-	-	-	-	-	-	-	-	-	-	-	-	-
age CH$_4$	YBP	-	-	-	-	-	6143 (6527)	-	13024 (8421)	2330 (15)	18155 (6710)	28240 (150)	-	-	-	-
age CO$_2$	YBP	-	-	-	-	-	2359 (1839)	-	833 (509)	585 (20)	3193 (180)	2545 (15)	-	-	-	-
n		-	-	-	-	-	14	-	3	1	2	1	-	-	-	-

*Estimated by ^{13}C model (section 3.5).
†n = 12 (removed outliers due to dissolution from long-term traps). Data shown as mean (std. dev. when n > 1, or measurement error when n = 1). G = GSL, D = Doughnut, C = Cranberry, S = Smith, V = Vault. Dashes = not measured. Ebullition data only from August 2015 bubble survey.

2.2.2. Collection of CH$_4$ and CO$_2$ From Open Water in Summer

During the summer (August 2015), we collected ebullition gases (bubbles; $n = 1$–14 per lake) from all lakes and dissolved gas ($n = 4$–10 per lake) at four of the lakes (Table 2). In GSL, we sampled ebullition gas at nine stations along a transect from its active thermokarst margin (eastern shoreline with rapid subsidence and erosion) to its passive margin ($n = 1$–2 samples per station). At five of these stations, we also collected dissolved gas: both at the water surface ($n = 5$) and near the lakebed ($n = 5$). Stations were selected where ebullition was prominent as opposed to following a predefined spatial gradient.

Ebullition gas was collected in passive, anchored bubble traps, submerged just below the surface but above point sources of ebullition. Rising bubbles displaced water in either inverted 2-L plastic bottles fitted with stopcocks or syringes with stopcocks fixed atop of funnel-shaped plastic skirts with cross-sectional openings of approximately 0.5 m^2 at their bases (Walter Anthony et al., 2012). Care was taken when anchoring bubble traps to minimize disturbance of sediments. If bubbles entered the traps as a result of the anchoring procedure, the traps were cleared such that any additional gas collection was natural. Once bottles or syringes had collected ample ebullition sample volume, we manually injected the collected gas into 37- or 58-ml, preevacuated glass serum bottles with blue butyl rubber stoppers (CLS-4209-14, Chemglass Life Sciences, Vineland, NJ, USA). Depending on the ebullition rate, gas was collected over time spans ranging from <10 min to 24 hr.

Dissolved gas samples were collected using an in situ dissolved gas concentration system following the methods in Elder et al. (2018). Water was pumped via a battery-powered peristaltic pump (Proactive Environmental Products, Alexis, Brandenton, FL, USA) at 1.2 L/min through a series of four filters: 178- and 40-μm stainless steel mesh (T-29595-39 and T-2959-35, Cole-Parmer, Vernon Hills, IL, USA), 20- and 5-μm 5″ polypropylene sediment depth filters (SD-25-0520 Flow-Pro and SD-25-0505 Hydronix, freshwatersystems. com, Greenville, SC, USA). The water then passed through a degassing membrane contactor (Liqui-Cel, Membrana, 3M, St. Paul, MN, USA), which rapidly equilibrated the dissolved gases across a microporous membrane, with an evacuated headspace. The extracted gases were desiccated and compressed into a custom-fabricated, preevacuated, preweighed 2-L stainless steel canister with stainless steel bellows sealed valves (SS-4BG, Swagelok, Solon, Ohio, USA). This method enables the collection of a sufficient mass of CH$_4$ and CO$_2$ (>0.1-mg C) for isotopic analysis in relatively low concentration waters (≥0.3 μM [CH$_4$] and/or [CO$_2$]). Between samples, particle filters were replaced, and the entire system was flushed for 30 min with the new sample water (about 40 L of water) to vent atmospheric air and

purge the system with new sample gas. After flushing, dissolved gas was diverted into the preevacuated canisters for 1 hr. All samples were shipped to UC Irvine and analyzed within 8 (dissolved gases) or 16 months (ebullition).

2.3. Laboratory Analysis of CO_2 and CH_4

2.3.1. Dissolved CH_4 and CO_2 Extraction for C Isotope Analysis

To extract dissolved gases from water samples collected in winter, we replaced the HDPE screw caps on the frozen 1.4-L water samples with 1N HCl acid-washed open-top polypropylene screw caps with custom fit 1/8″ thick butyl rubber septa and HDPE-lined silicone rubber septa in an ultrahigh purity (UHP) nitrogen (N_2) atmosphere. To preserve sample quality, the HDPE-lined septa were placed in contact with the sample. A 15% headspace of *zero air* (UHP, C-free air) was created in the 1.4-L bottles to ensure the highest sample yield to headspace ratio for extracting dissolved CH_4 (Yamamoto et al., 1976). Following 1 min of manual shaking and a 30-min rest period to allow bubble coalescence, headspace gases were completely evacuated into 2-L stainless steel canisters.

For isotope analysis, all CH_4 and CO_2 samples were purified on a flow-through vacuum system, and CH_4 was oxidized to CO_2 (see below). The stainless steel canisters, containing dissolved CH_4 and CO_2 collected in winter and summer, were balanced to atmospheric pressure with zero air to assist with the extraction process and to supply oxygen (O_2) to the in-line combustion of CH_4 to CO_2. We compared the canister mass before filling with the sample and balancing with UHP air to the canister mass after a 1-hr vacuum extraction to determine the efficiency of the extraction line. Highly concentrated samples were only extracted for 30 min, or after visual inspection of gas yields were high enough to terminate the extraction. The 1-hr extractions removed 92% ± 4% of the total canister volume on average, whereas the 30-min extractions removed an average of 56% ± 9%. For ebullition gases, aliquots ranging from 4 to 28 ml were removed from the glass serum bottles via syringe and directly injected into the flow-through vacuum system at a rate of approximately 4 ml/min.

The primary function of the flow-through vacuum extraction system is to separate and purify CH_4 and CO_2 from bulk gas samples (Pack et al., 2014). First, any sample-CO_2 is cryogenically isolated from CH_4, carbon monoxide (CO), and noncondensable gases, such as N_2. Next, sample-CO is combusted to CO_2 in a 290 °C furnace in the presence of cupric oxide (CuO) and cryogenically isolated. Then, any sample-CH_4 is quantitatively combusted at 950 °C, also in the presence of CuO, and the resulting water vapor and CO_2 are isolated. If sample-CO_2 and/or CH_4-derived CO_2 yields were >0.2 mg C, an aliquot was taken for $\delta^{13}C$ analysis via isotope ratio mass spectrometry (GasBench II, DeltaPlus XL, Thermo Fisher Scientific, Pittsburgh, PA, USA). Sample CO_2 and CH_4-derived CO_2 were then chemically reduced to graphite for ^{14}C analysis via accelerator mass spectrometry (AMS) (Xu et al., 2007). All isotope analysis was conducted at the W. M. Keck Carbon Cycle AMS (KCCAMS) Laboratory at UC Irvine.

2.3.2. CH_4 and CO_2 Concentration Analysis

The concentration of summer dissolved CH_4 was determined via a headspace equilibration technique (Magen et al., 2014), where headspace-CH_4 concentrations were measured via gas chromatography and a flame ionization detector (Shimadzu, GC-2014, Addison, Illinois, USA) at UA Fairbanks' Water and Environmental Research Center. Methane concentrations were verified with gas standards ranging from 15.1 ppm to 60% CH_4. Calibration curves were linear across the entire standard gas range ($R^2 = 1$, $n = 3$, SCOTTY gas calibration standards, Air Liquide Specialty Gases LLC, Plumsteadville, PA, USA). Summer concentrations of dissolved CO_2 were estimated based on previously observed Liqui-Cel extraction efficiencies (about 4% in Arctic lakes; Elder et al., 2018) for dissolved CO_2 and the vacuum line extraction yields. The concentrations of below-ice-dissolved CH_4 and CO_2, and CH_4 and CO_2 in ebullition gas samples, were estimated on the basis of vacuum-extraction yields and calculated headspace and extraction efficiencies. Extraction efficiencies for dissolved CH_4 and CO_2 in winter 2015 were not determined, rendering the concentration estimates for that sample set ($n = 6$) unusable; however, this has no effect on our isotopic assays since each sample was completely extracted.

Based on results from Greene et al. (2014), where dissolved CH_4 concentrations were monitored on a monthly basis over 2 years in GSL, we assume that our measurements in late August and late March or April represent CH_4 concentrations close to both the annual minima and maxima, respectively. August

measurements represent a dissolved CH_4 pool drawn down by oxidation and ventilation over the course of the open-water period. March/April measurements represent a period after dissolved O_2 has been completely consumed, and CH_4 diffusing from sediments and from ice-trapped ebullition has accumulated in the water column during ice cover and before spring thaw (Greene et al., 2014).

2.4. Quantification of Annual Ebullition Rates on GSL

For GSL only, annual ebullition rates were estimated by quantifying the density of predefined ebullition seep types (A, B, C, and Hotspot) using ice-bubble surveys as in Walter Anthony and Anthony (2013). A fifth seep type, known as *tiny seeps*, which are small, widely dispersed, and unmerged in lake ice (Greene et al., 2014; Lindgren et al., 2016), were also quantified. Walter Anthony and Anthony (2013) also show the locations of these surveys on GSL, which covered aproximately 10% of the lake area. Seep densities are then multiplied by seep-type-specific, long-term ebullition rates, measured year round using submerged bubble traps. This transfer function is described in detail in Walter Anthony and Anthony (2013) and provides an accurate volumetric ebullition flux value for GSL. Once volumetric ebullition rates are accurately known, a mass-based estimate of CH_4 ebullition is made based on lake-and-seep-specific measurements of CH_4 concentrations using gas chromatography (Shimadzu, GC-2014, Addison, Illinois, USA) at the Water and Environmental Research Center. The methods of ebullition gas collection from bubble traps and subsequent CH_4 concentration analysis are described in detail in Walter et al. (2008).

To estimate the additions of below-ice CH_4 to the dissolved pool in GSL, we used the annual proportion of ebullition-CH_4 entering the dissolved pool (26%) estimated by Greene et al. (2014). This quantity is only added during the ice-covered period (approximately 220 days on GSL; Greene et al., 2014; Lindgren et al., 2016) and allows for estimation of the daily addition rate below ice. Since ice-on and ice-off dates were not recorded in this study, the same ice duration and period as observed in Greene et al. (2014; winter 2012/2013) was applied to our calculations. We expect this has negligible impact on our main conclusions relative to the variability in isotopic observations, measurements, and their associated uncertainties.

2.5. Seasonal Water Volume Estimation Using Bathymetry Data

A three-dimensional model of GSL bed topography was created using a triangular irregular network (TIN) model in ArcGIS, which used Delaunay triangulation criterion for approximately 6,000 bathymetric points. These points were collected during a prior study using a Humminbird 798ci sonar unit with integrated GPS sensor and 200/83-kHz beams mounted on a boat. Summer and winter water volumes (19,740 and 15,520 m^3, respectively) were estimated from the model by creating artificial planes in the TIN at desired depth intervals. Further, the volumes of the hyperlimnion and hypolimnion (11,300 and 8,440 m^3) were determined for stratified summer conditions. For this we assumed a thermocline depth of 1.25 m below the surface (Greene et al., 2014). In winter, we reduced the below-ice water volume by the thickness of maximum black ice growth, which we assumed to be 0.45 m (Greene et al., 2014). Since this study did not determine the interannual volume fluctuation of GSL, we prescribed a static lake level for all lake volume determinations. This likely contributes a small source of error in our estimates of whole-lake CH_4 and CO_2 concentrations and the subsequent mass balance calculations. A hypothetical volume fluctuation of $\pm15\%$ in GSL would have negligible impact on our modeled results (<1% change) and main conclusions, suggesting a relative indifference to a fluctuating lake volume.

2.6. Sources of Dissolved CH_4 and CO_2

When ice is not present, ebullition-CH_4 has negligible interaction with the dissolved CH_4 pool (Greene et al., 2014). Thus, in summer the dissolved CH_4 pool represents a combination of diminishing amounts of CH_4 from previously trapped winter sources (Greene et al., 2014; Phelps et al., 1998), CH_4 diffusing from lake sediments (Tan et al., 2015), and any dissolved CH_4 imported from the watershed (Lecher et al., 2017). Given the continual processing and ventilation of CH_4 throughout the open-water season, we assume the dissolved CH_4 at the time of measurement at the end of summer (late August) to be solely representative of CH_4 concurrently imported from the watershed or diffusing from lake sediments. Although diffusive sources to lake dissolved CH_4 and CO_2 pools are likely to vary in origin and magnitude throughout the year, our analysis does not differentiate diffusive sources from one another; rather, they are conceptually grouped and differentiated only from ebullition sources. Despite the likely interannual variability in watershed and

lake-sediment sources of dissolved CH_4 and CO_2, we posit that given the prior work conducted by Greene et al. (2014) and results presented herein, intra-annual variations in these source variations are negligible relative to the drastic seasonal effect of ice trapping and forcing the dissolution and oxidation of large quantities of ebullition-CH_4 within the water column. Since GSL's watershed is almost completely frozen in winter, we assert that the dissolved pool at the end of summer (August) integrates the majority of the thaw-season watershed influence on dissolved ^{14}C variability. We assume that any further changes to the ^{14}C signatures of dissolved CH_4 and CO_2 are predominantly the result of ice trapping and forcing ebullition-CH_4 to dissolve into the unfrozen water column and oxidation of large quantities of this dissolved gas into CO_2.

On an annual basis, seasonal ice on GSL forces approximately 26% of all ebullition-CH_4 to dissolve into the water column (Greene et al., 2014). During the ice-cover period, 55% of all ebullition is impeded by ice. Of this quantity, 20% of the impeded CH_4 is encased by ice and the remaining 80% dissolves into water (Greene et al., 2014). Therefore, the below-ice dissolved CH_4 pool in late winter (March/April) is a time-and-mass-integrated representation of all winter dissolved CH_4 sources in the lake water column.

2.7. Determining the Whole-Lake ^{14}C Age of CH_4 Ebullition

We compared three independent methods for estimating the integrated whole-lake ^{14}C age of CH_4 ebullition in GSL.

2.7.1. Bubble Surveys

Ebullition is highly sporadic in space and time (Bastviken et al., 2004; Lindgren et al., 2016; Sepulveda-Jauregui et al., 2015; Wik, Thornton, et al., 2016), and bubbles vary greatly in CH_4 and CO_2 concentration and isotopic content (Brosius et al., 2012; Walter et al., 2008). Therefore, to estimate the whole-lake integrated ^{14}C signature of ebullition in GSL, we used the concentration of CH_4 in 10 bubble gas seeps in summer as a weighting factor for averaging the whole-lake ^{14}C age of CH_4 ebullition. Since we assume that CH_4 concentration in bubbles is a proxy for the bubble-CH_4-flux magnitude, weighting the ^{14}C signatures in each observed seep by its respective CH_4 concentration preserves the mass-balanced ^{14}C signature of integrated whole-lake CH_4 ebullition. Two anomalously low ebullition-CH_4 concentration values are not reported and were not used in ^{14}C weighting. The anomaly was likely due to the combined effect low ebullition rates from these seeps and longer-term placement (>24 hr) of these bubble traps allowing gas exchange with the water column before samples were collected. Removal of these low-concentration weights altered the concentration-weighted ^{14}C value by only 2%; thus, the affect was considered negligible for the conclusions of this work.

We then compared our concentration-weighted 10-seep estimate from August 2015 to a previous and more comprehensive, multiyear survey of annual CH_4 emissions (Greene et al., 2014; Walter Anthony et al., 2010) and ^{14}C age of 30 seeps in GSL (Walter Anthony et al., 2016). We assume that this more comprehensive mean ^{14}C signature and flux is representative of average annual ebullition on GSL. For this method, seep categories and their associated fluxes were classified by the system developed by Walter Anthony et al. (2010) and applied in Greene et al. (2014). Along with an estimation of the annual ebullition flux, the ^{14}C of CH_4 were previously and separately analyzed by Walter Anthony et al. (2016) in the 30 seeps and averaged for each seep category. Mean $^{14}CH_4$ signatures for each seep category were weighted by their respective annual rates and then summated to derive a flux-weighted whole-lake ^{14}C signature for ebullition-CH_4 in GSL. For comparison to winter dissolved $^{14}CH_4$ methods herein, we excluded the flux and ^{14}C signature of the strongest CH_4 ebullition hot spots, which are capable of periodically maintaining an open hole in winter ice and thus are not always trapped nor forced to dissolve into the water column. Including open-hole CH_4 ebullition in the flux-weighted calculation shifted the estimated mean ^{14}C age of whole-lake ebullition older by approximately 18%, or 1,090 ^{14}C years. Methods that only assess the below-ice dissolved CH_4 pool to understand whole-lake ebullition are only partially sensitive to *open-hole* hot spot emissions since bubble-CH_4 would only interact with the dissolved pool during periodic freeze-over of open holes in very cold weather. The following interpretation of the dissolved pool considers the losses of open-hole ebullition-CH_4 as a source of error (around $\pm1,100$ ^{14}C years) in our estimates of whole-lake ^{14}C of ebullition-CH_4.

2.7.2. Open Water Versus Ice-Covered $^{14}CH_4$ End-Members and ^{14}C-Based Mass Balance of CH_4 Oxidation to CO_2

We developed a novel approach, independent from ebullition-based ^{14}C analysis, to provide a comparative estimate the whole-lake integrated ^{14}C signature of ebullition. The observed seasonal differences in dissolved $^{14}CH_4$ and $^{14}CO_2$ were interpreted as mass-dependent alterations made by the mixing of ice-trapped ebullition into the dissolved pool and CH_4 oxidation to CO_2. During both of these processes, ^{14}C signatures are conserved on the principle of mass balance, allowing for quantification of seasonal fluxes and the ^{14}C signature of whole-lake ebullition.

The total moles and mean ^{14}C signatures of dissolved CH_4 and CO_2 were estimated in GSL in August 2015 ($n = 10$) and March 2016 ($n = 8$). A ^{14}C-based, two end-member mass balance was used to determine the effect of oxidation of ^{14}C-distinct CH_4 (older) to CO_2 (younger) beneath the ice:

$$^{14}CO_{2\ Mar} = f_{ox\ 14C}\left(^{14}CH_{4\ Mar}\right) + (1 - f_{ox\ 14C})\left(^{14}CO_{2\ Aug}\right) \tag{1}$$

where $^{14}CO_{2Mar}$ and $^{14}CO_{2Aug}$ are the concentration-weighted mean ^{14}C signatures of dissolved CO_2 in March 2016 and August 2015, respectively. $^{14}CH_{4Mar}$ is the concentration-weighted mean below-ice signature of dissolved CH_4 in March, and $f_{ox\ 14C}$ is the fraction of $^{14}CO_{2Mar}$ composed of the C from oxidized, below-ice dissolved CH_4 ($^{14}CH_{4Mar}$). Since aerobic respiration of organic material is expected to be low in the oxygen poor sediments, this model assumes that below-ice CH_4 oxidation is the only process that changes the whole-lake ^{14}C signature of the dissolved CO_2 pool below ice.

Solving equation (1) for $f_{ox\ 14C}$ and multiplying it by the total moles of CO_2 in GSL in March (CO_{2Mar}) provides our estimate of total CH_4 oxidation to CO_2 below ice in moles (CH_{4ox}):

$$CH_{4\ ox} = f_{ox\ 14C}(CO_{2\ Mar}) \tag{2}$$

To approximate the total CH_4 additions to the dissolved pool below ice (CH_{4total}), $CH_{4\ ox}$ is added to the net increase in total moles of dissolved CH_4 between August 2015 (CH_{4Aug}) and March 2016 (CH_{4Mar}):

$$CH_{4\ total} = CH_{4\ ox} + \left(CH_{4\ Mar} - CH_{4\ Aug}\right) \tag{3}$$

The fraction of trapped and dissolved ebullition-CH_4 comprising the below ice CH_4 pool (f_{eb}) is approximated by dividing 26% of the annual ebullition flux (see above and Greene et al., 2014, for estimation of annual additions to the dissolved pool by ebullition during ice cover) by CH_{4total}:

$$f_{eb} = \frac{0.26(\text{annual } CH_4 \text{ ebullition})}{CH_{4\ total}} \tag{4}$$

This fraction (f_{eb}) is then used in another two end-member ^{14}C mass balance to determine the integrated whole-lake ^{14}C signature of ebullition-CH_4 ($^{14}CH_{4ebullition}$):

$$^{14}CH_{4\ ebullition} = \frac{^{14}CH_{4\ Mar} - (1 - f_{eb})\left(^{14}CH_{4\ Aug}\right)}{f_{eb}} \tag{5}$$

where $^{14}CH_{4Aug}$ is the concentration-weighted mean ^{14}C signature of dissolved CH_4 in August and $^{14}CH_{4Mar}$ is as in equation (1). Since CH_4 dissolution from trapped bubbles dominates that from sediments (Greene et al., 2014), this model assumes that below-ice dissolution of trapped ebullition-CH_4 is the only process that alters the ^{14}C signature of the dissolved CH_4 pool from the open-water August value.

2.7.3. Dissolved CH_4 Keeling Plot Intercept

Lastly, we used a Keeling plot approach (Pataki et al., 2003) to assess the integrated mean age of the strongest C sources to the dissolved CH_4 and CO_2 pool during the winter and summer. This approach plots the reciprocal of CH_4 concentration for each sample on the x axis against its ^{14}C value on the y axis. A linear regression is computed and the resulting y intercept represents the ^{14}C value of the primary CH_4 or CO_2 source. Similar to the models above, this method assumes linear mixing of two sources by the principle of mass balance, that is, lake-sediment C sources versus trapped ebullition-CH_4 dissolving into the water column

below ice. Since ^{13}C is sensitive to oxidation/consumption dynamics of CH_4, and we did not devise an experiment to test pathway-dependent ^{13}C differences in ebullitive versus diffusive CH_4, we do not use the Keeling plot method with ^{13}C to distinguish ebullition CH_4 from diffusive CH_4 at the end of the ice cover period when oxygen has been consumed. The Keeling plot linear regressions were calculated using a Deming function, where the error in both the CH_4 concentration data and their associated ^{14}C values was incorporated into determining the error in the calculated y intercept. We consider the Keeling plot regressions significant at the standard $\alpha = 0.95$ level. In winter, we assume that the Keeling intercept represents the spatially and temporally integrated whole-lake-^{14}C signature of trapped ebullition-CH_4 dissolving into the water column, since ebullition is typically highly concentrated in CH_4. In summer, this value represents the C source that contributes the most CH_4 to the dissolved pool.

2.8. Multiple C Sources for Whole-Lake Ebullition

Since whole-lake integrated ebullition (winter Keeling Plot y intercept value) represents a combination of CH_4 produced and bubbled from various lake sources of different age (lake sediment C and permafrost C), we used a probabilistic multisource model to estimate the relative CH_4 contribution from multiple ^{14}C end-member categories (Phillips & Gregg, 2003):

$$FM_S = f_A FM_A + f_B FM_B + f_C FM_C + f_D FM_D \quad 1 = f_A + f_B + f_C + f_D \tag{6}$$

FM_S is the ^{14}C signature of integrated whole-lake ebullition ^{14}C as determined by the Keeling plot approach in winter. Four distinct categories were chosen based on the mean ^{14}C signatures of the five ebullition seep categories described above (FM_{A-D} correspond to tiny seeps, A + B seeps, C seeps, and hot spots). Although A and B seeps have different flux rates on GSL, their ^{14}C signatures are approximately the same. Therefore, they were combined into one source category for this analysis. The relative proportions of each of the sources (seep category) to the observed FM_S are symbolized by f_{A-D}.

2.9. Dissolved CH_4 Oxidation Models, Based On ^{13}C

Since the concentration of dissolved CH_4 at any point in the year represents a balance between production and consumption, and these quantities were not directly observed, stable C isotope (^{13}C) mass balance models were used to estimate dissolved CH_4 consumption between the April 2015 and August 2015 sampling periods. During microbial oxidation of dissolved CH_4 in the water column, $^{12}CH_4$ is slightly favored over $^{13}CH_4$, resulting in a kinetic isotope fractionation factor (α_{ox}) of 1.037 (equation7; Kankaala et al., 2007). This value was empirically derived in a boreal lake similar to GSL and thus was appropriate for our approximations:

$$\alpha_{ox} = \frac{k_{12}}{k_{13}} \tag{7}$$

where k_{12} and k_{13} are the first-order rate constants for the consumption of $^{12}CH_4$ and $^{13}CH_4$, respectively.

Following the methods and assumptions of the Rayleigh distillation equations in (Coleman et al., 1981), we used a ^{13}C-based closed-system model to estimate the fraction of dissolved CH_4 that is consumed between its assumed annual maxima (April 2015) and annual minima (August 2015) in GSL ($f_{ox\ closed}$):

$$f_{ox\ closed} = 1 - \frac{m_{Aug}}{m_{Mar}} = 1 - e^{\left[\frac{\delta^{13}CH_{4\ Aug} - \delta^{13}CH_{4\ Mar}}{1000\left(\frac{1}{\alpha_{ox}} - 1\right)}\right]} \tag{8}$$

where m_{Aug} and m_{Mar} are the total moles of dissolved CH_4 in GSL in August and March and $\delta^{13}CH_{4Aug}$ and $\delta^{13}CH_{4Mar}$ are the ^{13}C values in ‰ of dissolved CH_4 in GSL in August and March relative to the international ^{13}C standard, Vienna Pee Dee Belemnite. The kinetic fractionation factor of CH_4 oxidation is denoted by α_{ox} (see above). Although the CO_2 produced from below-ice CH_4 oxidation likely remains in the system until GSL ventilates during spring thaw, CH_4 is continuously added from sediments and trapped-bubble dissolution, meaning that the lake is not a purely closed system. Thus, the closed-system Rayleigh distillation can only roughly estimate CH_4 consumption between the two sampling periods.
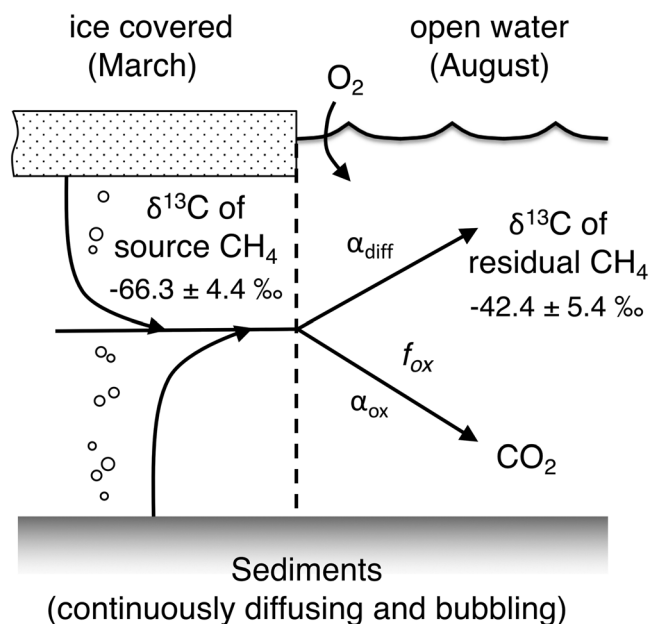
Figure 1. Simplified scheme of open-system CH_4 oxidation and associated ^{13}C dynamics in a seasonally ice-covered lake. Methane production is dominant in ice-cover conditions, but once the lake is ventilated during spring melt, CH_4 flow reaches a branch point and either evades oxidation and escapes the system or is oxidized to CO_2 in the water column. Adapted from Blair et al. (1985) and Liptay et al. (1998)). $\delta^{13}C$ values in the figure represent the mean ± std. dev. of March 2015 ($n = 3$) and August 2015 ($n = 10$) dissolved CH_4.

To more closely approximate the semiopen/open system of GSL between March and August, we also used an approach detailed in Liptay et al. (1998), where oxidation of CH_4 in a *flow through system* was estimated in landfill cover soils:

$$f_{\text{ox open}} = \frac{\delta^{13}CH_{4\,\text{Aug}} - \delta^{13}CH_{4\,\text{Mar}}}{1000(\alpha_{ox} - \alpha_{\text{diff}})} \quad (9)$$

where f_{oxopen} is the fraction of the original CH_4 substrate (annual maxima in April 2015) that is consumed and α_{diff} is the fractionation factor of CH_4 diffusion, determined to equal 1.001 in permafrost-affected water-saturated sediments (Preuss et al., 2013). Isotopic fractionation in dynamic flow-through or open-systems, such as this, requires a division of substrate flow (CH_4 oxidation in this case), also known as a branch point (Blair et al., 1985). Analogous to landfill cover soils, the branch point in lakes occurs where CH_4 emitted from sediments or dissolving ice-trapped bubbles is either oxidized in the water column or is not oxidized and leaves the system (emitted to atmosphere; Figure 1). Like the closed-system model, this approach assumes first-order reaction kinetics for the oxidation of CH_4 to CO_2 and both also assume steady state conditions. Since residual $^{13}CH_4$ was not significantly different between stratified surface and bottom waters of GSL in summer (equally enriched by oxidation), we believe that O_2 was not a limiting factor in CH_4 oxidation during our summer survey, and thus, the assumption of CH_4-based first-order kinetics is valid. Although previous work has found O_2-limited CH_4 oxidation in surface waters of GSL in the summer (one out of five O_2-limited lakes from 25 total study lakes in Martinez-Cruz et al., 2015), this study asserts that evidence of $^{13}CH_4$ enrichment in both surface and deep waters of GSL is enough to validate the rough estimate provided by the open-system model. Additionally, recent studies have also found evidence for higher-than-expected methanotrophy at low oxygen concentrations in permafrost ponds (Crevecoeur et al., 2017) and alpine lakes (Blees et al., 2014), suggesting that CH_4 consumption may be primarily influenced by the concentration of CH_4 substrate and thus consistent with first-order kinetics. Since we did not measure dissolved O_2 in this study, we acknowledge these assumptions as sources of error in our estimates of seasonal CH_4 consumption.

3. Results and Discussion

3.1. Dissolved CH_4 and CO_2 Concentrations

In GSL, both dissolved CH_4 and CO_2 were saturated with respect to atmospheric equilibrium by a minimum of 580 times for CH_4 and 34 times for CO_2 throughout the 2-year study (Table 2). Similarly, the other four study lakes were supersaturated in CH_4 and CO_2 at each sampling event, and there was a trend toward decreasing dissolved gas concentrations and lower ratios of CH_4 to CO_2 with increasing lake size (Tables 1 and 2). Although lake-to-atmosphere fluxes were not determined, we assume that the supersaturation of both CH_4 and CO_2 meant that all lakes were sources of these gases to the atmosphere when ice was not prohibitive.

In all lakes during summer, dissolved CH_4 concentration differences between surface water and water near the lakebed were indicative of thermal stratification. In GSL, surface water had over 60 times lower mean CH_4 concentrations (5.9 ± 2.0 μM, $n = 5$) than water near the lake bed (367.6 ± 240.9 μM, $n = 4$, single outlier = 1,956.7 μM; Figure 2a). The summer average dissolved CH_4 concentration in GSL was 160.5 ± 16 μM when accounting for the distinct concentrations and volumes of each layer. These concentration estimates are within the range previously reported for GSL, both above and below the thermocline (Greene et al., 2014). Summer dissolved CO_2 concentrations in GSL varied between 543 and 997 μM (mean = 615 μM, $n = 8$) and were well mixed. These CO_2 concentration estimates are within the range
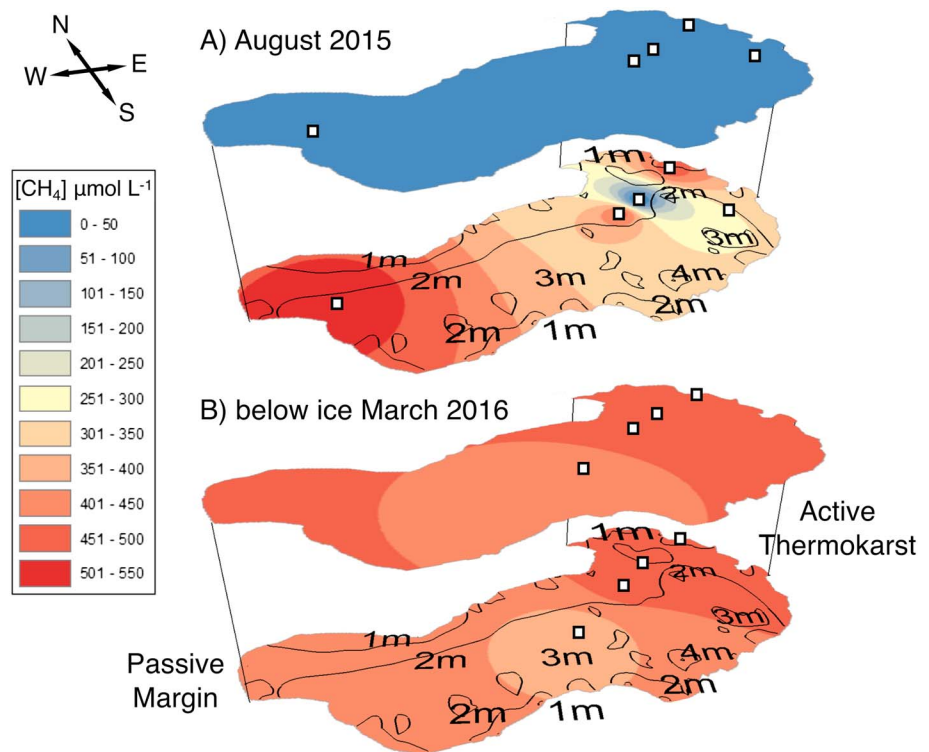
Figure 2. Concentration of dissolved CH_4 in Goldstream Lake in open water conditions of August 2015 (A) and beneath floating ice in March of 2016 (B). White squares mark sampling locations. Black lines and depth labels in the bottom layers show the bathymetry of the lake. Interpolated values were determined via inverse distance weighting in ESRI, ArcMap with the default power value equal to two. Class breaks of equal intervals were chosen to span the range of observed CH_4 concentrations.

reported approximately 50 cm below the thermocline during the same month (August) in GSL (Gonzalez-Valencia et al., 2014).

Below-ice, dissolved CH_4 and CO_2 were more concentrated than in summer (Table 2). In GSL, dissolved CH_4 concentrations were 3 times greater in winter, averaging 458 ± 46 μM (Table 2) and were more homogeneous with respect to lake depth than in summer (Figure 2b). Winter dissolved CO_2 concentrations (638 ± 141 μM, 2016) were also well mixed, as in summer. Our below-ice total moles of CH_4 and CO_2 estimation accounted for estimated water volume reduction from seasonal black-ice growth. Since ice thickness was not measured in this study, we applied the peak black-ice thickness that was observed in GSL during the winters of 2011 and 2012 (0.45 m; Greene et al., 2014). We estimate that water volume reduction could explain up to 17% of the below-ice CH_4 concentration increase between sampling periods. This effect was considered in our mass balance estimates of the whole-lake $^{14}CH_4$ of ebullition and produced <5% variation in the results.

These seasonal trends largely held true in the four other lakes studied. In August 2015, concentrations ranged from 3 to 574 μM for dissolved CH_4 and 658 to 1,988 μM for CO_2 (Table 2). Concentrations of both gases, and the CH_4 to CO_2 ratio, decreased in summer as a function of increasing lake size (from 0.3 and 0.6 in Vault Lake and GSL to 0.005 and 0.004 in Doughnut and Smith Lakes, respectively). Dissolved CH_4 increased in winter by 12,000% and 300% in Doughnut and Smith Lake, respectively, and CO_2 concentrations showed no seasonal change in Doughnut Lake. However, CO_2 concentrations decreased by 80% in Smith Lake in winter. Other than Smith Lake's dissolved CO_2, the accumulation of gas in winter shows the clear influence of ice impeding emissions to the atmosphere.

Our sampling design captured the seasonal amplitude of the dissolved CH_4 pool. We observed a minimum of 3,170 moles of dissolved CH_4 in August 2015 and a maximum of 7,110 moles CH_4 in March 2016 in GSL,
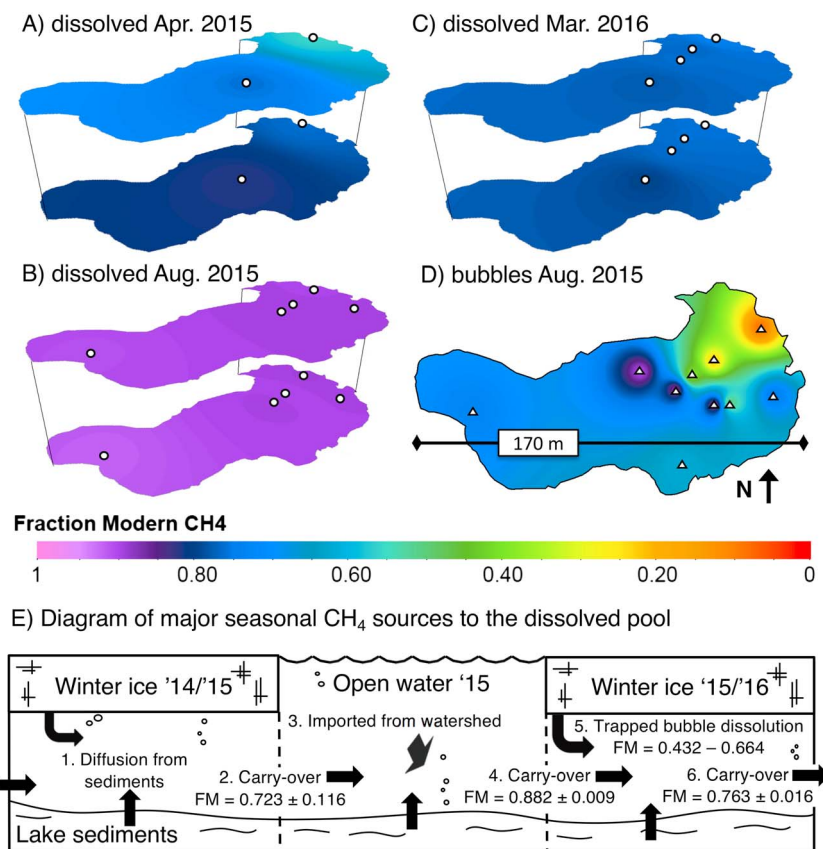
Figure 3. [14]C signature (in Fraction Modern) of dissolved CH_4 in Goldstream Lake in below-ice conditions in winter 2015 (A), open-water in summer 2015 (B), below-ice in winter 2016 (C), and ^{14}C of ebullition CH_4 from 10-seep survey in August of 2015 (D). White circles indicate dissolved CH_4 sampling locations (A–C) and white triangles mark sampled ebullition seeps (D). Interpolated values were determined via inverse distance weighting in ESRI, ArcMap with the default power value equal to two. A custom color ramp was used to clearly illustrate the heterogeneity of ebullition relative to dissolved CH_4. Major seasonal sources to the dissolved CH_4 pool in GSL with mean [14]CH_4 values in Fraction Modern where measured (in no particular order; E).

which is similar to previous observations (Greene et al., 2014). If we assume that this seasonal difference is a result of ebullition-CH_4 entering the dissolved CH_4 pool below ice, we can estimate the flux of ebullition during the ice-covered period. Our estimate (3,940 moles of dissolved CH_4) is within 5% of expected wintertime additions to the dissolved pool estimated from previous work on GSL (Greene et al., 2014), which provided an estimate of annual CH_4 ebullition, and the proportions of which are added to the water column below ice (3,710 moles of CH_4).

3.2. [14]C Ages of CH_4 and CO_2

In GSL, the ^{14}C signatures of dissolved CH_4 and CO_2 were relatively uniform across the lake (Figure 3. and Table 2). In summer 2015, the ^{14}C age of dissolved CH_4 across GSL ranged only 290 ^{14}C years ($n = 10$), a relative standard deviation (RSD) <9%. Winter [14]CH_4 ages ranged only 570 ^{14}C years in 2015/2016 ($n = 8$, RSD <8%); however, winter 2014/2015 ages ranged 3,100 ^{14}C years ($n = 4$, RSD = 50%) since one sample was an outlier (2x older than the mean of all below-ice [14]CH_4 measurements in GSL). Similarly, the ^{14}C age of dissolved CO_2 in GSL varied by 510, 75, and 35 ^{14}C years in winter 2014/2015, summer 2015, and winter 2015/2016, respectively.

Dissolved [14]CH_4 ages ranged from modern to 4,730 YBP across all lakes, whereas dissolved CO_2 ranged from modern to 3,515 YBP (Table 2). In all lakes, both dissolved CH_4 and CO_2 were older during the ice-cover period than during the open-water period ($P < 0.05$, $n = 4$, 14, and 8 for April 2015, August 2015, and

March 2016, respectively; Table 2). The dissolved C pools tended to be older in smaller lakes and lakes with more active thermokarst (see below). In GSL, dissolved $^{14}CH_4$ ages were not significantly different in winter 2014/2015 versus winter 2015/2016 ($P > 0.05$); however, dissolved $^{14}CO_2$ was older by an average of 443 ^{14}C years in winter 2015/2016 versus winter 2014/2015 ($P < 0.05$, $n = 8$ and 4, respectively). This is likely due to interannual variation in the age of dissolved DIC imported from the watershed as opposed to variation in $^{14}CH_4$ oxidation since the ages of $^{14}CH_4$ ages did not vary significantly amongst the two winter observation periods.

Across all study lakes, the age of CH_4-C in bubbles was older on average and more variable (395 ± 15 to $28,240 \pm 150$ YBP) than that of the dissolved pool (modern to $4,730 \pm 170$ YBP), regardless of season or measurement year (Table 2). Since we only measured $^{14}CH_4$ in one winter ebullition sample from GSL, we are unable to directly determine the interannual variability of the ^{14}C age of ebullition.

Although we did not directly asses these processes, we hypothesize that the observed $^{14}CH_4$ age difference between bubbles and dissolved $^{14}CH_4$ could be explained by the fact that bubbles are more likely to form and dislodge from deeper sediments, where methanogenesis acts on older C substrates and where the partial pressure of produced CH_4 exceeds the hydrostatic pressure of the surrounding pore water (Siegel et al., 2001). This CH_4 partial pressure excess is more likely to occur in deeper regions of sediments where dissolved nitrogen comprises less of the total partial pressure of dissolved gasses (Eilrich, 2002). Alternatively, younger dissolved CH_4 is also likely diffusively imported from the surrounding watershed (E3 in Figure 3.), which is likely influenced by inputs of relatively young and fresh organic material for methanogenesis (Lecher et al., 2017), thus lowering the overall age of the dissolved CH_4 relative to concurrent ebullition. Finally, observed diffusion of CH_4 from northern lake environments originated from material fixed from labeled CO_2 as recent as 2 hr before the observed flux (King et al., 2002). Although King et al. (2002) did not study ebullition, their results imply that diffusional CH_4 sources can be amongst the youngest within the lake environment.

Our ebullition observations are consistent with previous ^{14}C surveys of ebullition in interior Alaska and emissions from yedoma lakes in Siberia (Douglas et al., 2016; Walter Anthony et al., 2010; Walter et al., 2006, 2008). Ebullition-CH_4 was also always older than ebullition-CO_2 ages (70 to 7,470 YBP), regardless of season, and was not significantly different between lake sizes. Although equal quantities of CH_4 and CO_2 are produced during the methanogen pathway of acetate fermentation, the observed age discrepancy is likely a result of the less soluble CH_4 gas-forming bubbles in sediments, dislodging, and entraining younger CO_2 during its ascent through talik and lake sediments.

In GSL, the ^{14}C age of CH_4-Cin bubbles increased with proximity to the active thermokarst margin (eastern shoreline; Figure 3.d). This result was also observed in Brosius et al. (2012) and supports the finding that thawing Pleistocene permafrost contributes to CH_4 emissions in thermokarst lakes (Walter Anthony et al., 2016). The high spatial variation in ^{14}C age of ebullition-CH_4 within GSL demonstrates the utility of an integrative dissolved-based approach to assess the whole-lake ^{14}C age of ebullition-CH_4.

Together, our concentration and isotope data confirmed that floating ice cover results in efficient mixing of typically older ebullition CH_4 into the more homogeneous dissolved CH_4 pool during winter (Greene et al., 2014). Thus, measurements of dissolved $^{14}CH_4$ in winter can be used as a proxy for whole-lake-integrated CH_4 emissions, facilitate lake-to-lake comparisons, and can be used to assess sources of CH_4 across regional scales.

3.3. Oxidation of CH_4 to CO_2, Determined With ^{13}C and ^{14}C

A ^{14}C mass balance estimated that approximately $50\% \pm 5\%$ of the below-ice dissolved CO_2 (in March 2016) originated as oxidized dissolved CH_4. We used this fraction (f_{ox14C} in equation (1)) and the total number of moles of dissolved CO_2 in GSL in March 2016 ($CO_{2Mar} = 9,910 \pm 1,980$ moles CO_2) to determine that $4,970 \pm 1,100$ moles of CH_4-derived CO_2 (with the concentration-weighted ^{14}C signature of below-ice dissolved CH_4, $^{14}CH_{4Mar}$ FM = 0.763 ± 0.016) is needed to shift the whole lake ^{14}C signature of CO_2 from the value observed in August 2015 ($^{14}CO_{2Aug}$FM = 0.919 ± 0.002) to that of March of 2016 ($^{14}CO_{2Mar}$FM = 0.841 ± 0.001). This assumes that CH_4 conversion to CO_2 is the only modifier to the ^{14}C signature of the dissolved CO_2 pool below ice, or in other words, that the ^{14}C signature of whole-lake

sources to dissolved CO_2 in August is relatively constant compared to the distinct additions of ice-trapped ebullition-CH_4 to the water column. A hypothetical sensitivity analysis was performed to determine the effect of a variable summer dissolved $^{14}CO_2$ value on our calculations. The fluctuation of $^{14}CO_{2Aug}$ by $\pm 20\%$ (approximately 140 ^{14}C years) altered the resulting fraction of oxidized CH_4 ($f_{ox\ 14C}$) and the total below-ice CH_4 addition by only $\pm 5\%$. This suggests that oxidation of ^{14}C-distinct below-ice CH_4 is the dominant process that alters the intra-annual ^{14}C signature of below-ice dissolved CO_2 from its open-water value. We then estimated a total addition rate in GSL of 43 ± 2 mol CH_4 lake^{-1} d^{-1} to the dissolved pool between August 2015 and March 2016 by adding the moles of CH_4 converted to CO_2 ($4,970 \pm 250$ mol CH_4) to the net increase in total dissolved moles of CH_4 between August and March ($3,940 \pm 200$ mol CH_4; equation (3)) and dividing by the number of days between sampling (206 days). Also, using the quantity of CH_4 converted to CO_2, we determined the CH_4 consumption rate to be 0.020 ± 0.001-mg CH_4 L^{-1} d^{-1} when averaged over the entire period between sampling, or 0.050 ± 0.003-mg CH_4 L^{-1} d^{-1} if dissolved O_2 is depleted within the first 60 days of ice cover, as suggested by Greene et al. (2014). The latter CH_4 consumption rate is very similar to previous estimates of winter CH_4 oxidation in GSL and other yedoma lakes in Alaska (Martinez-Cruz et al., 2015). Considering additions and losses of CH_4 to the dissolved pool between August 2015 and March 2015 (ice-cover period), we determined the net CH_4 accumulation rate in GSL to be 19 mol CH_4 lake^{-1} d^{-1}. Together, we determined that $56\% \pm 5\%$ of all CH_4 added to the dissolved pool by ebullition between August and March is converted to CO_2. This quantity is remarkably equal to the proportion of ebullition-derived dissolved CH_4 that is consumed by methanotrophy (56%), estimated by Greene et al. (2014), which used monthly observations and CH_4 oxidation models. Interannual variation in open-water sources to dissolved CH_4 and CO_2 could affect the proportions of CH_4 oxidized or ebullition-CH_4 dissolved in our modeled calculations; however, since these variations are integrated into end-of-summer ^{14}C signatures of both dissolved gases, they are indirectly incorporated into modeled parameters for the following ice-cover period.

The total dissolved CH_4 addition rate between August 2015 and March 2016 sampling (43 ± 2 mol CH_4 lake^{-1} d^{-1}) was approximately 2 times greater than our estimate of the expected additions solely from ice-trapped ebullition to the dissolved pool (21 mol CH_4 lake^{-1} day^{-1}). This implies that CH_4 diffusion from sediments comprised roughly half of the total CH_4 additions to the dissolved pool between the August and March measurement periods (mostly ice-cover period).

We also used the mean $\delta^{13}CH_4$ values observed below-ice in GSL in April 2015 ($-66.3\% \pm 4.4\permille$) and open-water in August 2015 ($-42.4 \pm 5.4\permille$) to approximate the fraction of the dissolved CH_4 pool that was consumed by methanotrophy throughout the open-water period ($f_{ox\ closed}$ & $f_{ox\ open}$). GSL was considered as a semi-closed system in winter, when ice cover partially impedes CH_4 ebullition, and as an open system in summer. Using a closed-system Rayleigh distillation, we estimated a $49\% \pm 28\%$ drawdown of the April 2015 dissolved CH_4 pool measured over the summer ($f_{ox\ closed}$, equation (8)), or $66 \pm 44\%$ using an open-system model ($f_{ox\ open}$, equation (9)). Despite the significant difference between dissolved April 2015 and August 2015 $\delta^{13}CH_4$ values ($P < 0.05$), both ^{13}C models are highly sensitive to the initial and residual $\delta^{13}C$ values, and thus exhibit large errors when the standard deviations of the open water versus ice-covered mean $\delta^{13}CH_4$ considered. Therefore, the modeled quantities should be considered as rough estimates. Although dissolved CH_4 concentrations were not determined in April of 2015, and CH_4 addition rates were not determined throughout the open-water period, we used August 2015 concentrations and the total fraction of CH_4 consumed from the ^{13}C models to estimate that roughly 4,300 moles of dissolved CH_4 were consumed between April 2015 and August 2015. This corresponds to an average CH_4 consumption rate of 0.03-mg CH_4 L^{-1} d^{-1}, which is an order of magnitude less than summer CH_4 oxidation rates previously determined for surface water of GSL but more closely resembles that of other nonyedoma lakes in the same study (Martinez-Cruz et al., 2015). Since surface water oxidation rates are likely much higher than those at depth, and because our estimate is based on ^{13}C observations at the lake's surface and bottom waters, we would expect lower overall rates of CH_4 consumption when compared to surface-only observations as in Martinez-Cruz et al. (2015). We regard the relatively large errors in the two ^{13}C models as conservative; however, given their general agreement and the similarity of their results to previous work, they are still useful for estimating seasonal CH_4 consumption when sampling is infrequent.

3.4. Integrated ^{14}C Age of Whole-Lake CH$_4$ Ebullition

3.4.1. Whole-Lake Integrated ^{14}C-Age of Ebullition via Bubble Surveys

In the August 2015 bubble survey in GSL, we estimated the concentration-weighted mean value of ^{14}C in bubble-CH$_4$a s FM = 0.457 ($n = 14$), or approximately 6,290 YBP (Figure 3.d). In a more comprehensive past bubble survey, which is complementary to our August 2015 data set, the whole-lake, flux-weighted mean value of ^{14}C in bubble-CH$_4$ from GSL ranges from FM = 0.432 to 0.495, depending on the proportion of open-hole hotspots seeps included in the estimate. This corresponds to a ^{14}C age range of 6,740 to 5,660 YBP. The range in mean concentrations of CH$_4$ in bubbles from the August 2015 survey (44.8–93.7%, $n = 19$ across all study lakes, Table 2) were within ranges reported from other circumpolar lakes (Walter et al., 2008), but were more variable and generally lower than previously observed ebullition on GSL (82%–89%, $n = 246$; (Walter Anthony & Anthony, 2013). This discrepancy may be the result of sampling during periods of low atmospheric pressure in August 2015, where samples could have incorporated more N$_2$-rich gas from shallower sediments (Walter et al., 2008).

Although both bubble surveys cumulatively quantified ^{14}CH$_4$ in 40 seeps, ranging from the smallest measurable to those with the largest flux magnitudes on GSL, it is impossible to directly asses the full variability in ^{14}C-distinct fluxes in ebullition-CH$_4$ across an entire lake whose seeps number in the thousands. For example, despite a relatively comprehensive estimate of tiny seep flux rates on GSL, only one ^{14}C measurement was made on this seep category (FM = 0.985 $\pm$ 0.001). This relatively modern signature, and the fact that tiny seep ebullition comprises 20% of whole-lake ebullition in our estimate, means that tiny seeps have significant weight on the integrated whole-lake ^{14}C age of ebullition. Hypothetically, if tiny seeps represented 0% of whole-lake CH$_4$ ebullition, then the adjusted ^{14}C age would be approximately 11,000 YBP as opposed to 6,740-5,660 YBP when tiny seeps are included.This effect may be somewhat counterbalancedby the propensity of bubble surveys to detect and sample (especially for ^{14}C) the stronger and more apparent seeps, which also tend to be older.Altogether, this may bias bubble surveys towards older integrated whole-lake values. Future efforts to characterize whole-lake ebullition should incorporate strategies to quantify sporadic tiny seep categories and the processes that produce them.

3.4.2. Mass Balance Approach to ^{14}C Signature of Whole-Lake Ebullition-CH$_4$

We also estimated the whole-lake ^{14}C signature of ebullition-CH$_4$ in GSL using a two-end member mass balance equation (equation (5)). Here we estimate the integrated ^{14}C signature of ebullition required to lower the ^{14}C of below ice dissolved CH$_4$ from the solely diffusive source signature (observed during open water, ^{14}CH$_{4Aug}$, E4 in Figure 3.) to the integrated ebullition-CH$_4$+ diffusive-CH$_4$ signature (observed below ice, ^{14}CH$_{4Mar}$, E6 in Figure 3.). The fraction of ^{14}CH$_{4Mar}$ sourced by ebullition-CH$_4$ (f_{eb} in equation (5), E5 in Figure 3.) was estimated to be 50% $\pm$ 5%. This fraction represents the proportion of the below-ice dissolved CH$_4$ originating from diffusion of trapped ebullition into the below-ice water column and was determined by dividing the expected ebullition-dissolution flux by the total observed additions (i.e., 21 mol CH$_4$ lake^{-1} day $^{-1}$ of 43 total mol CH$_4$ lake^{-1} day^{-1}). The other 50% $\pm$ 5% is assumed to originate from sediment diffusion. Using this approach, we found that the ^{14}C signature of whole-lake ebullition (FM = 0.643, or 3,550 ^{14}C YBP) approximately agreed with the value estimated by the Keeling plot intercept (FM = 0.612 $\pm$ 0.050, or 3,940 $\pm$ 660 ^{14}C YBP; see below). This result suggests that the simplistic Keeling plot approach is effective for estimating the integrated whole-lake ^{14}C signature of ebullition CH$_4$ in Boreal yedoma lakes and avoids tedious monitoring efforts required by ice-bubble surveys and associated ^{14}C analysis of the full spectrum of ebullition seep types. Seasonal CH$_4$ mass balance parameters are summarized in Table 3. Although this approach assumes that the dissolution of trapped ebullition is the only factor that can change the below-ice dissolved ^{14}CH$_4$ pool, a hypothetical sensitivity analysis that varied the summer concentration-weighted mean dissolved ^{14}CH$_4$ (^{14}CH$_{4Aug}$) by $\pm$20% (equal to a $\pm$ fluctuation of approximately 200 ^{14}C years), only resulted in a $\pm$4% change in the calculated ^{14}C signature of whole-lake CH$_4$ ebullition. This suggests that in GSL, a two-end-member model effectively describes the open water versus ice-covered shift in ^{14}C in the dissolved CH$_4$ pool.

3.4.3. Keeling Plot Analysis of Dissolved CH$_4$ and CO$_2$

Both open water (August 2015) and below-ice (March 2016) ^{14}CH$_4$ signatures are linearly correlated with the inverse of their respective dissolved CH$_4$ concentrations ($R^2 = 0.49$ and 0.88 for open water and below ice, respectively; Figure 4). Both regressions are significant at the 0.95 confidence level ($P < 0.05$), which

Table 3
Summary of Goldstream Lake CH_4 and CO_2 Mass Balance Parameters

Open water to below ice				Below ice to open water			
Parameter	Isotope	Value	Units	Parameter	Isotope	Value	Units
$^{14}CO_{2Aug}$	^{14}C	0.919 ± 0.002	FM	$^{13}CH_{4Aug}$	^{13}C	-42.4 ± 5.4	‰
$^{14}CO_{2Mar}$	^{14}C	0.841 ± 0.001	FM	$^{13}CH_{4Mar}$	^{13}C	-66.3 ± 4.3	‰
$^{14}CH_{4Aug}$	^{14}C	0.882 ± 0.009	FM	α_{ox}	k_{12}/k_{13}	1.037	s^{-1}/s^{-1}
$^{14}CH_{4Mar}$	^{14}C	0.763 ± 0.016	FM	α_{diff}	k_{12}/k_{13}	1.001	s^{-1}/s^{-1}
$f_{ox\ 14C}$	N.A.	0.50 ± 0.05	mol mol^{-1}	$f_{ox\ closed}$	N.A.	0.49 ± 0.28	mol mol^{-1}
f_{eb}	N.A.	0.27–0.55	mol mol^{-1}	$f_{ox\ open}$	N.A.	0.66 ± 0.44	mol mol^{-1}
CH_{4ox}	N.A.	$4,970 \pm 1,100$	mol CH_4				
CH_{4total}	N.A.	$8,910 \pm 1,450$	mol CH_4				
Annual CH_4 Ebullition*	N.A.	$24,020 \pm 1,200$	mol CH_4/yr				
$CO_{2\ Aug}$	N.A.	$12,200 \pm 2,440$	mol CO_2				
$CO_{2\ Mar}$	N.A.	$9,910 \pm 1,980$	mol CO_2				
CH_{4Aug}	N.A.	$3,170 \pm 630$	mol CH_4				
CH_{4Mar}	N.A.	$7,110 \pm 710$	mol CH_4				

N.A. = not applicable. Errors are based on either the std. deviation of mean values, the propagated error when mean values are used in further calculation, or the range of solutions from independent methods.
*From sediments to the water column (updated from Greene et al., 2014; Sepulveda-Jauregui et al., 2015).

implies that in each season, CH_4 is predominantly mixing between a concentrated source and a diffuse background pool. Neither below-ice nor open water dissolved CO_2 concentrations are strongly correlated with their corresponding ^{14}C values ($R^2 < 0.36$). Therefore, we assume that a two-component mixing model cannot seasonally constrain the sources of dissolved CO_2.

During the summer, CH_4 diffusing from lake sediments is likely the primary source to the dissolved pool, as any ebullition during the open water period loses a negligible fraction of CH_4 during its unimpeded transport to the atmosphere. Thermal stratification of GSL in summer resulted in a far greater range of dissolved CH_4 concentrations compared to those in the preceding winter (Figure 2). However, the corresponding ^{14}C values of summer dissolved CH_4 were less variable than winter values and thus exhibit a weaker correlation in the Keeling plot analysis (Figure 4). The younger summer Keeling plot y intercept of dissolved CH_4 (FM = 0.885 ± 0.003, or 980 ± 30 YBP) likely reflects the ^{14}C signature of the decaying organic material in the lake sediments that are most conducive to methanogenesis. This may be due to combination of optimal temperatures, relative quality or freshness of the organic material, and favorable redox conditions. Less concentrated dissolved CH_4 samples were younger still in ^{14}C-age, likely indicative a mostly modern C
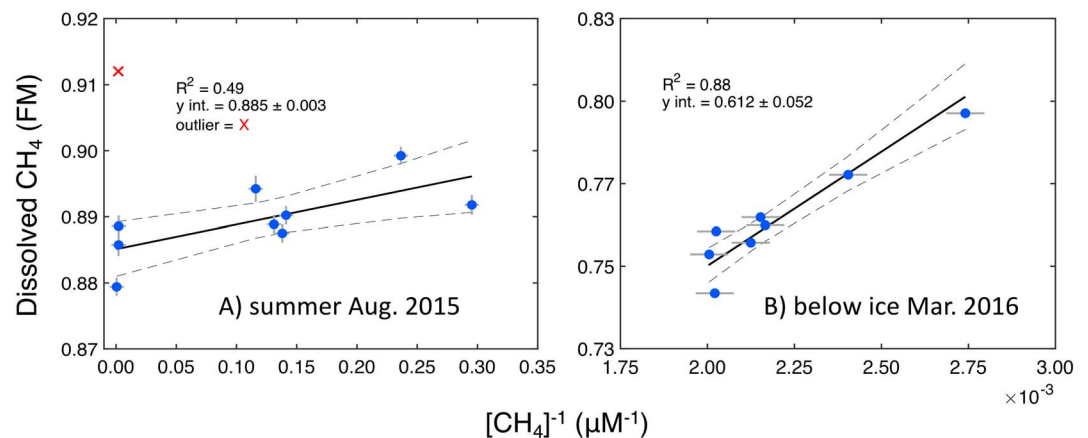

Figure 4. Keeling plot analysis of ^{14}C (shown as Fraction Modern (FM)) in dissolved CH_4 in open-water conditions in August 2015 (A) and in below-ice conditions in March of 2016 (B). Dashed lines represent the 0.95 C.I. Please note different FM values and concentrations scales in either season (x 10^{-3} only corresponds to x axis in B).

Table 4
Integrated Whole-Lake ^{14}C of Ebullition-CH_4 in GSL.

Method	*f_{eb} in Equation (5) %	Whole-lake age of Ebullition-CH_4 YBP
Bubble surveys	27–31	5,660–6,740
$^{14}CH_4$ oxidation & dissolution mass balance	50 ± 5	3,290–3,880
Keeling intercept	37–55	3,290–4,660

N.A. = not applicable.
*Fraction of winter dissolved CH_4 originating from ebullition.

source, such as CH_4 produced from recently photosynthesized C and imported from the watershed (Figure 4a). According to past ^{14}C-labeling experiments in arctic lakes, C from recent photosynthesis can be emitted as CH_4 from lake littoral zones within hours of assimilation (King et al., 2002). This offers another explanation for younger CH_4 ages observed in summer.

During ice cover, trapped ebullition-CH_4 dissolves and mixes with younger background CH_4 (sediment diffusion sources) at successively lower levels in less concentrated samples (Figure 4b). We interpret the winter Keeling plot y intercept (FM = 0.612 ± 0.052, or 3,940 ± 660 YBP) as the integrated whole-lake ^{14}C signature of ebullition-CH_4 and compare this value with that of the other methods above (Table 4). The extensive bubble survey method (5,660–6,740 YBP) agrees with the mean estimate from the less comprehensive August 2015 survey (6,290 YBP) but is between 1,780 and 3,450 ^{14}C years older than the estimates of whole-lake ebullition-CH_4 using either the $^{14}CH_4$ oxidation mass balance or winter Keeling plot y intercept methods. Of the three methods to assess the whole-lake ^{14}C signature of ebullition-CH_4, the Keeling plot method and the whole-lake ^{14}C oxidation mass balance have a greater ability to integrate all emission sources to the dissolved CH_4 pool than discrete bubble surveys. However, the methods that rely only on the dissolved CH_4 pool are not sensitive to any ebullition that passes through open holes in winter ice. As a result, our Keeling intercept and $^{14}CH_4$ oxidation methods may have estimated younger whole-lake ebullition-CH_4 ages due to through-ice ebullition of the oldest and strongest seeps within a lake. Furthermore, we assume an annually constant value for the flux-weighted and/or concentration-weighted whole-lake ^{14}C signatures of ebullition-CH_4. Intra-annual variability in the actual whole-lake ^{14}C signature of ebullition-CH_4, not captured by our bubble surveys, represents a potential source of error when this value is compared to the results of the mass balance approaches.

In the $^{14}CH_4$ oxidation mass balance model, the fraction of ebullition-CH_4 in the winter-dissolved pool was determined to be 50% ± 5%. This fraction (f_{eb} in equation 5) and the open water and ice-covered dissolved $^{14}CH_4$ end-members were used to estimate the whole-lake $^{14}CH_4$ signature of ebullition. In a similar way, the whole-lake $^{14}CH_4$ signatures of ebullition, as determined by the bubble surveys and by the Keeling plot method, were plugged into equation (5) to solve for f_{eb}. These results are summarized in Table 4.

Across all methods, the whole lake ^{14}C age of ebullition-CH_4 ranged from 3,270 to 6,740 YBP and the fraction of the below-ice dissolved pool, comprised of ebullition-CH_4, ranged from 27% to 55%. If tiny seeps were ignored in our bubble surveys, the whole-lake ^{14}C age of ebullition-CH_4 would be 11,030 ± 30 YBP; however, this would result in ebullition comprising <20% of below-ice dissolved CH_4. This fraction is considerably lower than that estimated by Greene et al. (2014), which showed that on annual basis, the dissolved CH_4 in GSL is comprised of 77% ebullition-CH_4. For comparison with our methods, a fraction of 77% would require a whole-lake ebullition-CH_4 age of 2,560 YBP, suggesting a stronger influence of smaller, younger, but more dispersed seeps (likely tiny seeps).Since the tiny seep-category is particularly difficult to quantify, especially for ^{14}C content, previous work could have suffered sampling bias towards the stronger and more observable seep categories, which have subsequently older ^{14}C ages.

3.5. Dominant C Pools for Methanogenesis

To further characterize the sources of whole-lake CH_4 emissions, we utilized an iterative four-source mass balance model (equation (6)) to estimate the range of possible contributions from four key C reservoirs in GSL. The four ^{14}C end-members were chosen based on the distinct seep types characterized by Lindgren
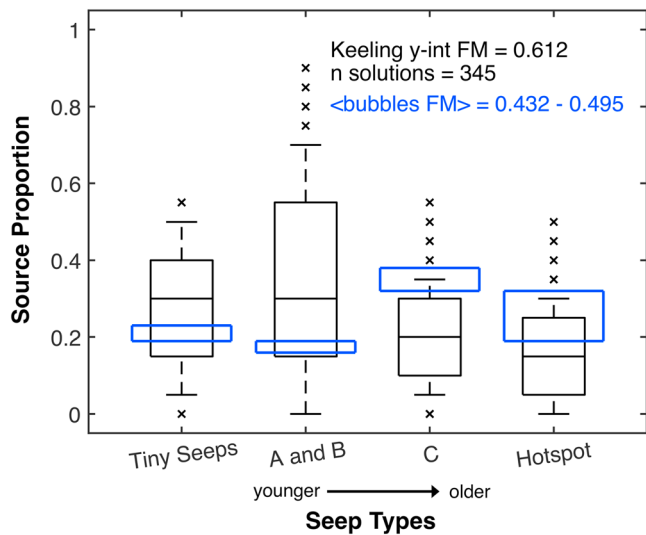
Figure 5. Seep apportionment to the whole-lake $^{14}CH_4$ of ebullition as determined by the Keeling plot intercept (black boxes and whiskers). Boxes enclose the IQR and show the median of mass balance solutions (345 potential solutions). Whiskers encompass the 10th –90th percentile range of mass balance solutions, and black x's show unlikely solutions falling outside this range. Source proportions determined by an iterative multi-source mass balance model (equation (6)). See text for description of ebullition sources: Tiny seeps, A and B seeps, C seeps, and Hotspot seeps. Blue boxes show the range in the relative contributions of each seep type to the flux-weighted whole-lake $^{14}CH_4$ of ebullition determined via bubble surveys.

et al. (2016) and Walter Anthony and Anthony (2013) and previously surveyed in a comprehensive study ($n = 30$). Seep categories included tiny seeps 120 ± 40 YBP ($n = 1$, analytical error only), A and B seeps (combined in this plot) $2,710 \pm 2590$ YBP ($n = 5$), C seeps $11,200 \pm 3,250$ YBP ($n = 3$), and weaker hotspot seeps still susceptible to blockage by winter ice $13,740 \pm 3,160$ YBP ($n = 21$).

Mass balance solutions were computed for the winter 2015 Keeling y intercept end-member (FM = 0.612 ± 0.05, or $3,940 \pm 660$ YBP; Figure 4b). Since the integrated mixture (Keeling y intercept) was 3,940 YBP, the younger C sources (tiny seeps, A and B) contributed the majority of CH_4 to the dissolved pool (Figure 5). The range in source contributions to the whole-lake ^{14}C signature of ebullition as in the bubble surveys (blue boxes in Figure5) were also computed and represent the inclusion of the upper limit of hotspot emissions, meaning that all hot spot emissions were trapped by ice. Increasing the quantity of hot spot emissions dissolving into the below-ice dissolved pool has the effect of reducing the relative contributions from the other seep types and increasing the ^{14}C age of whole-lake ebulltion-CH_4contributions to the dissolved pool by approximately 1,100 ^{14}C years. The two older C sources (C seeps and hot spot), combined, likely contributed less than half of the ebullition-CH_4 to the whole lake integrated CH_4 pool. The discrepancy between the whole-lake ^{14}C signatures estimated by the Keeling approach and the two bubble surveys may be a result of sampling bias during bubble surveys toward stronger, more apparent seeps that are easier to sample and typically older. In the case of bubble surveys conducted in the fall or early winter, sampled seeps may also be older since surface lake sediments have cooled, are less productive, and thus contribute less relatively young CH_4 to ebullition.

The spatial and temporal variability of ebullition presents challenges for characterizing whole-lake sources, thus the Keeling plot approach, which integrates all sources during the months-long ice-cover season, has several advantages over bubble surveys.
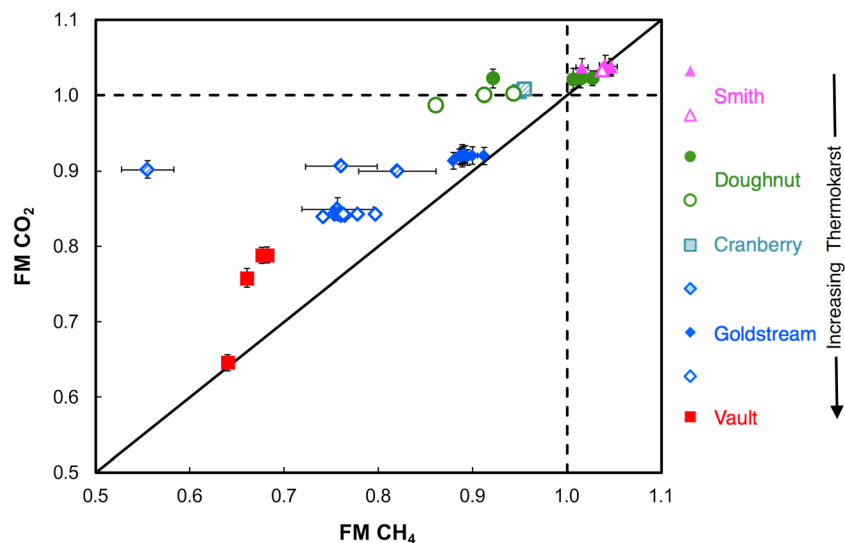

Figure 6. Seasonal and regional variability in the ^{14}C of dissolved CH_4 and CO_2 in five lakes in Interior Alaska, shown as Fraction Modern (FM). Filled symbols represent samples taken during open water conditions in August 2015, open symbols represent measurements made under ice in March 2016, and open symbols with hashes represent measurements made under ice in April of 2015. Samples containing ^{14}C from nuclear weapons testing post calendar year 1950 have FM > 1. The lake legend is ranked from top to bottom in order of increasing thermokarst activity.

3.6. Regional and Open Water Versus Ice-Covered Variability in Dissolved $^{14}CH_4$ and $^{14}CO_2$

Although this study primarily focused on GSL, characterization of ^{14}C in dissolved CH_4 and CO_2 of four other lakes in the Fairbanks region elucidated a pattern between dissolved gas age and thermokarst activity. Regardless of the season, ^{14}C of dissolved CH_4 and CO_2 were oldest in lakes with the greatest amounts of active thermokarst (Figure 6). This finding represents an important qualitative relationship for lake-to-lake comparisons of the environmental factors that control lakes' ability to access and emit ancient permafrost C. This finding is also consistent with recent work stating that CH_4 emissions from lakes are proportional to permafrost C thaw from thermokarst (Walter Anthony et al., 2016).

The strong correlation in CH_4 and CO_2 ^{14}C values across lakes demonstrates that both gases originate from similar sources on the regional level and that lakes process large quantities of CH_4 to CO_2. Although highly correlated (Figure 6), CH_4 ages tend to be slightly older than those of CO_2. Additionally, age offsets between the two gases appear to be greatest in the winter, when ice traps older ebullition CH_4 and forces it into the dissolved pool. Together, this correlation and seasonal pattern also demonstrate that large quantities of CH_4 released from lake sediments are converted to CO_2 before they are emitted to the atmosphere. In this case, the trapping effect of ice on thermokarst lakes regulates the global warming impact of lake-GHG emissions by increasing the time in which CH_4 is vulnerable to the oxidative water column.

4. Conclusions

This study used C isotopes to investigate the seasonal dynamics of CH_4 and CO_2 emissions from climate-sensitive northern lakes in the Boreal zone of interior Alaska. We showed that winter ice is an integrating mechanism for whole-lake emission sources of CH_4. Furthermore, we developed, tested, and compared conceptual models for understanding the relative proportions and sources of CH_4 diffusion, ebullition, and oxidation to CO_2 in the regionally representative lake, GSL.

This work also showed that the presence of ice impeded CH_4 ebullition and forced approximately half of below-ice ebullition-CH_4 to be oxidized in our primary study lake. The other half accumulated in the dissolved pool under ice, only to be oxidized or ventilated to the atmosphere over the course of the open-water season. Together, this demonstrates the importance of seasonal ice in regulating the global warming impact of GHG emissions from thermokarst lakes. If warming reduces the duration of ice cover on northern lakes, the ratio of annual CH_4 to CO_2 emissions is likely to increase and thus accelerate further climate warming and ice-cover decline.

This research also showed a clear relationship between thermokarst activity and whole-lake ^{14}C age of CH_4 and CO_2 emissions, consistent with the hypothesis that where warming climates induce further thermokarst activity in ice-and-C-rich permafrost, large quantities of ancient permafrost C are likely to be released to the atmosphere. Furthermore, if thawed anaerobic zones expand as a result of thermokarst, and less ebullition is trapped during shorter ice-cover periods, significant portions of this ancient C release are likely to be as CH_4, strengthening the warming impact of thermokarst.

This work demonstrates that isotopic measurements of the dissolved CH_4 and CO_2 pools, from spring (annual maximum) to summer (annual minimum) to the following spring (annual maximum), can elucidate the integrated whole-lake emission sources and pathways in thermokarst lakes. We conclude that the Keeling plot approach is the most effective means for determination of the whole-lake ^{14}C signature of ebullition when sampling size is representative of diverse lake properties and large enough to produce a statistically significant linear regression. A larger seasonal difference in the ^{14}C ages of dissolved CH_4 and CO_2 likely imply either a greater influence of ebullition in whole-lake emissions and/or ebullition originating from much older sources than those of the dissolved pools. Once CH_4 and CO_2 emission sources are known on the whole-lake scale, interlake relationships can be assessed on spatial scales relevant to remote sensing, land models, and efforts to constrain future circumpolar C emissions and how they will feed back to global climate. To further understand circumpolar emissions of ancient C as CH_4 and/or CO_2 from climate-sensitive thermokarst lakes, broader regional surveys of whole-lake emissions should be conducted to capture the complexity of Arctic and boreal lake types. Surveys should incorporate broad geomorphological and climatological variability (from tundra thermokarst to periglacial kettle ponds),

diffusive versus ebullition dominated systems, and the diversity of soil and sedimentary C pools found across the circumpolar region.

References

Bastviken, D., Cole, J., Pace, M., & Tranvik, L. (2004). Methane emissions from lakes: Dependence of lake characteristics, two regional assessments, and a global estimate. *Global Biogeochemical Cycles*, *18*, GB4009. https://doi.org/10.1029/2004GB002238

Blair, N., Leu, A., Muñoz, E., Olsen, J., Kwong, E., & Des Marais, D. (1985). Carbon isotopic fractionation in heterotrophic microbial metabolism. *Applied and Environmental Microbiology*, *50*(4), 996–1001.

Blees, J., Niemann, H., Wenk, C. B., Zopfi, J., Schubert, C. J., Kirf, M. K., et al. (2014). Micro-aerobic bacterial methane oxidation in the chemocline and anoxic water column of deep south-Alpine Lake Lugano (Switzerland). *Limnology and Oceanography*, *59*(2), 311–324. https://doi.org/10.4319/lo.2014.59.2.0311

Brosius, L. S., Walter Anthony, K. M., Grosse, G., Chanton, J. P., Farquharson, L. M., Overduin, P. P., & Meyer, H. (2012). Using the deuterium isotope composition of permafrost meltwater to constrain thermokarst lake contributions to atmospheric CH_4 during the last deglaciation. *Journal of Geophysical Research*, *117*, G01022. https://doi.org/10.1029/2011JG001810

Coleman, D. D., Risatti, J. D., & Schoell, M. (1981). Fractionation of carbon and hydrogen isotopes by methane-oxidising bacteria. *Geochimica et Cosmochimica Acta*, *45*, 1033–1037.

Crevecoeur, S., Vincent, W. F., Comte, J., Matveev, A., & Lovejoy, C. (2017). Diversity and potential activity of methanotrophs in high methane-emitting permafrost thaw ponds. *PLoS ONE*, *12*(11), 1–22. https://doi.org/10.1371/journal.pone.0188223

Denfeld, B. A., Baulch, H. M., del Giorgio, P. A., Hampton, S. E., & Karlsson, J. (2018). A synthesis of carbon dioxide and methane dynamics during the ice-covered period of northern lakes. *Limnology and Oceanography Letters*, *3*, 117–131. https://doi.org/10.1002/lol2.10079

Douglas, P. M. J., Stolper, D. A., Smith, D. A., Walter Anthony, K. M., Paull, C. K., Dallimore, S., et al. (2016). Diverse origins of Arctic and Subarctic methane point source emissions identified with multiply-substituted isotopologues. *Geochimica et Cosmochimica Acta*, *188*, 163–188. https://doi.org/10.1016/j.gca.2016.05.031

Eilrich, B. (2002). Formation and transport of CH4 and CO2 in deep peatlands Isotope geochemical analysis and numerical modelling based on field research at the Etang de la Gruère Bog in Switzerland (Doctoral Dissertation). Retrieved from RERO DOC Digital Library. (OAI identifier: oai:doc.rero.ch:20051011135750-JH).

Elder, C. D., Xu, X., Walker, J., Schnell, J. L., Hinkel, K. M., Townsend-Small, A., et al. (2018). Greenhouse gas emissions from diverse Arctic Alaskan lakes are dominated by young carbon. *Nature Climate Change*, *8*(2), 166–171. https://doi.org/10.1038/s41558-017-0066-9

Gonzalez-Valencia, R., Magana-Rodriguez, F., Gerardo-Nieto, O., Sepulveda-Jauregui, A., Martinez-Cruz, K., Walter Anthony, K. M., et al. (2014). In situ measurement of dissolved methane and carbon dioxide in freshwater ecosystems by off-axis integrated cavity output spectroscopy. *Environmental Science and Technology*, *48*(19), 11,421–11,428. https://doi.org/10.1021/es500987j

Greene, S., Walter Anthony, K. M., Archer, D., Sepulveda-Jauregui, A., & Martinez-Cruz, K. (2014). Modeling the impediment of methane ebullition bubbles by seasonal lake ice. *Biogeosciences*, *11*(23), 6791–6811. https://doi.org/10.5194/bg-11-6791-2014

Heslop, J. K., Walter Anthony, K. M., Sepulveda-Jauregui, A., Martinez-Cruz, K., Bondurant, A., Grosse, G., & Jones, M. C. (2015). Thermokarst-lake methanogenesis along a complete talik profile. *Biogeosciences*, *12*(6), 4865–4905. https://doi.org/10.5194/bgd-12-4865-2015

Kankaala, P., Taipale, S., Nykänen, H., & Jones, R. I. (2007). Oxidation, efflux, and isotopic fractionation of methane during autumnal turnover in a polyhumic, boreal lake. *Journal of Geophysical Research*, *112*, G02003. https://doi.org/10.1029/2006JG000336

King, J. Y., Reeburgh, W. S., Thieler, K. K., Kling, G. W., Loya, W. M., Johnson, L. C., & Nadelhoffer, K. J. (2002). Pulse-labeling studies of carbon cycling in Arctic tundra ecosystems: The contribution of photosynthates to methane emission. *Global Biogeochemical Cycles*, *16*(4), 1062. https://doi.org/10.1029/2001GB001456

Kling, G. W., Kipphut, G. W., & Miller, M. C. (1991). Arctic lakes and streams as gas conduits to the atmosphere: implications for tundra carbon budgets. *Science (New York, N.Y.)*, *251*(4991), 298–301.

Lecher, A. L., Chuang, P., Singleton, M., & Paytan, A. (2017). Sources of methane to an Arctic Lake in Alaska: An Isotopic Investigation. *Journal of Geophysical Research: Biogeosciences*, *122*, 753–766. https://doi.org/10.1002/2016JG003491

Lindgren, P. R., Grosse, G., Anthony, K. M. W., & Meyer, F. J. (2016). Detection and spatiotemporal analysis of methane ebullition on thermokarst lake ice using high-resolution optical aerial imagery. *Biogeosciences*, *13*, 27–44. https://doi.org/10.5194/bg-13-27-2016

Liptay, K., Chanton, J., Czepiel, P., & Mosher, B. (1998). Use of stable isotopes to determine methane ocidation in landfill cover soils. *Journal of Geophysical Research*, *103*(D7), 8243–8250.

Magen, C. C., Lapham, L. L., Pohlman, J. W., Marshall, K., Bosman, S., Casso, M., & Chanton, J. P. (2014). A simple headspace equilibration method for measuring dissolved methane. *Limnology and Oceanography: Methods*, *12*, 637–650. https://doi.org/10.4319/lom.2014.12.637

Martinez-Cruz, K., Sepulveda-Jauregui, A., Walter Anthony, K. M., & Thalasso, F. (2015). Geographic and seasonal variation of dissolved methane and aerobic methane oxidation in Alaskan lakes. *Biogeosciences*, *12*(15), 4595–4606. https://doi.org/10.5194/bg-12-4595-2015

Matveev, A., Laurion, I., Deshpande, B. N., Bhiry, N., & Vincent, W. F. (2016). High methane emissions from thermokarst lakes in subarctic peatlands. *Limnology and Oceanography*, *61*(S1), S150–S164. https://doi.org/10.1002/lno.10311

Muhs, D. R., & Budahn, J. R. (2006). Geochemical evidence for the Origin of Late Quaternary Loess in Central Alaska. *Canadian Journal of Earth Sciences*, *43*(3), 323–337. https://doi.org/10.1139/E05-115

Murton, J. B., Goslar, T., Edwards, M. E., Bateman, M. D., Danilov, P. P., Savvinov, G. N., et al. (2015). Palaeoenvironmental interpretation of yedoma silt (ice complex) deposition as cold-climate Loess, Duvanny Yar, Northeast Siberia. *Permafrost and Periglacial Processes*, *26*(3), 208–288. https://doi.org/10.1002/ppp.1843

Myhre, G., Shindell, D., Bréon, F.-M., Collins, W., Fuglestvedt, J., Huang, J., et al. (2013). Anthropogenic and Natural Radiative Forcing. In T. F. Stocker, D. Qin, G.-K. Plattner, M. Tignor, S. K. Allen, J. Boschung, et al. (Eds.), *Climate Change 2013: The Physical Science Basis. Contribution of Working Group I to the Fifth Assessment Report of the Intergovernmental Panel on Climate Change* (pp. 659–740). Cambridge, United Kingdom and New York, NY, USA: Cambridge University Press.

Pack, M. a., Xu, X., Lupascu, M., Kessler, J. D., & Czimczik, C. I. (2014). A rapid method for preparing low volume CH_4 and CO_2 gas samples for 14C AMS analysis. *Organic Geochemistry*, *78*, 89–98. https://doi.org/10.1016/j.orggeochem.2014.10.010

Pataki, D. E., Ehleringer, J. R., Flanagan, L. B., Yakir, D., Bowling, D. R., Still, C. J., et al. (2003). The application and interpretation of Keeling plots in terrestrial carbon cycle research. *Global Biogeochemical Cycles*, *17*(1), 1022. https://doi.org/10.1029/2001GB001850

Phelps, A., Peterson, K., & Jeffries, M. (1998). Methane effiux from high-latitude lakes during spring ice melt. *Journal of Geophysical Research*, *103*, 29,029–29,036.

Phillips, D. L., & Gregg, J. W. (2003). Source partitioning using stable isotopes: coping with too many sources. *Oecologia*, *136*(2), 261–269. https://doi.org/10.1007/s00442-003-1218-3

Preuss, I., Knoblauch, C., Gebert, J., & Pfeiffer, E. M. (2013). Improved quantification of microbial CH_4 oxidation efficiency in arctic wetland soils using carbon isotope fractionation. *Biogeosciences*, *10*(4), 2539–2552. https://doi.org/10.5194/bg-10-2539-2013

Sepulveda-Jauregui, A., Walter Anthony, K. M., Martinez-Cruz, K., Greene, S., & Thalasso, F. (2015). Methane and carbon dioxide emissions from 40 lakes along a north–south latitudinal transect in Alaska. *Biogeosciences*, *12*(11), 3197–3223. https://doi.org/10.5194/bg-12-3197-2015

Serreze, M. C., & Barry, R. G. (2011). Processes and impacts of Arctic amplification: A research synthesis. *Global and Planetary Change*, *77*(1–2), 85–96. https://doi.org/10.1016/j.gloplacha.2011.03.004

Siegel, D. I., Chanton, J. R., Glaser, P. H., Chasar, L. S., & Rosenberry, D. O. (2001). Estimating methane production rates in bogs and landfills by deuterium enrichment of pore water. *Global Biogeochemical Cycles*, *15*(4), 967–975. https://doi.org/10.1029/2000GB001329

Tan, Z., Zhuang, Q., & Walter Anthony, K. M. (2015). Modeling methane emissions from arctic lakes: Model development and site-level study. *Journal of Advances in Modeling Earth Systems*, *7*, 459–483. https://doi.org/10.1002/2014MS000314

Walter Anthony, K. M., & Anthony, P. (2013). Constraining spatial variability of methane ebullition seeps in thermokarst lakes using point process models. *Journal of Geophysical Research: Biogeosciences*, *118*, 1015–1034. https://doi.org/10.1002/jgrg.20087

Walter Anthony, K. M., Anthony, P., Grosse, G., & Chanton, J. (2012). Geologic methane seeps along boundaries of Arctic permafrost thaw and melting glaciers. *Nature Geoscience*, *5*(6), 419–426. https://doi.org/10.1038/ngeo1480

Walter Anthony, K. M., Daanen, R., Anthony, P., Schneider Von Deimling, T., Ping, C. L., Chanton, J. P., & Grosse, G. (2016). Methane emissions proportional to permafrost carbon thawed in Arctic lakes since the 1950s. *Nature Geoscience*, *9*, 679–682. https://doi.org/10.1038/ngeo2795

Walter Anthony, K. M., Vas, D., Brosius, L., Chapin, F. III, Zimov, S., & Zhuang, Q. (2010). Estimating methane emissions from northern lakes using ice-bubble surveys. *Limnology and Oceanography: Methods*, *8*, 592–609.

Walter, K. M., Chanton, J. P., Chapin, F. S., Schuur, E. A. G., & Zimov, S. A. (2008). Methane production and bubble emissions from Arctic lakes: isotopic implications for source pathways and ages. *Journal of Geophysical Research*, *113*, G00A08. https://doi.org/10.1029/2007JG000569

Walter, K. M., Zimov, S. A., Chanton, J. P., Verbyla, D., & Chapin, F. S. (2006). Methane bubbling from Siberian thaw lakes as a positive feedback to climate warming. *Nature*, *443*(7107), 71–75. https://doi.org/10.1038/nature05040

Wik, M., Thornton, B. F., Bastviken, D., Uhlbäck, J., & Crill, P. M. (2016). Biased sampling of methane release from northern lakes: A problem for extrapolation. *Geophysical Research Letters*, *43*, 1256–1262. https://doi.org/10.1002/2015GL066501

Wik, M., Varner, R. K., Walter Anthony, K. M., MacIntyre, S., & Bastviken, D. (2016). Climate-sensitive northern lakes and ponds are critical components of methane release. *Nature Geoscience*, *9*(2), 99–106. https://doi.org/10.1038/ngeo2578

Xu, X., Trumbore, S. E., Zheng, S., Southon, J. R., McDuffee, K. E., Luttgen, M., & Liu, J. C. (2007). Modifying a sealed tube zinc reduction method for preparation of AMS graphite targets: Reducing background and attaining high precision. *Nuclear Instruments and Methods in Physics Research Section B: Beam Interactions with Materials and Atoms*, *259*(1), 320–329. https://doi.org/10.1016/j.nimb.2007.01.175

Yamamoto, S., Alcauskas, J. B., & Crozier, T. E. (1976). Solubility of methane in distilled water and seawater. *Journal of Chemical & Engineering Data*, *21*(1), 78–80. https://doi.org/10.1021/je60068a029

Zimov, S. A., Voropaev, Y. V., Semiletov, I. P., Davidov, S. P., Prosiannikov, S. F., Chapin, F. S., et al. (1997). North Siberian Lakes: A methane source fueled by pleistocene carbon. *Science (New York, N.Y.)*, *277*(5327), 800–802. https://doi.org/10.1126/science.277.5327.800